Design, fabrication and performance evaluation of a compact regenerative evaporative cooler: towards low energy cooling for buildings

Zhiyin Duan[a*], Xudong Zhao[b], Junming Li[c]

[a] Beijing Key Lab of Heating, Gas Supply, Ventilating and Air Conditioning Engineering, Beijing University of Civil Engineering and Architecture, Beijing 100044, China

[b] University of Hull, Hull, HU6 7RX, UK

[c] Key Laboratory for Thermal Science and Power Engineering of Ministry of Education, Department of Thermal Engineering, Tsinghua University, Beijing 100084, China

Abstract

The urges of reducing energy use and carbon footprint in buildings have prompted the developments of regenerative evaporative coolers (RECs). However, the physical dimensions of RECs have to be designed enormous in order to deliver a large amount of supply airflow rate and cooling capacity. To tackle the issue, this paper develops a large-scale counter-flow REC with compact heat exchanger through dedicated numerical modelling, optimal design, fabrication and experimentation. Using modified ε-NTU method, a finite element model is established in Engineering Equation Solver environment to optimise the cooler's geometric and operating parameters. Based on modelling prediction, the cooler's experimental prototype was optimally designed and constructed to evaluate operating performance. The experiment results show that the cooler's attained wet-bulb effectiveness ranges from 0.96 to 1.07, the cooling capacity and energy efficiency ratio from 3.9 to 8.5 kW and 10.6 to 19.7 respectively. It can provide sub-wet bulb cooling while operating at high intake channel air velocities of 3.04-3.60 m/s. The superiority of proposed cooler's performance is disclosed by comparing with different RECs under similar operating conditions. Both the cooler's cooling capacity per unit volume and per unit airflow rate are found to be 62-108% and 21.6% higher respectively.

Keywords:

Indirect evaporative cooling; Dew point cooling; Heat and mass exchanger; Experimental and numerical investigations

1. Introduction

[*] Corresponding author. Tel: +86 10 68322535

E-mail address: duanzhiyin@bucea.edu.cn (Z. Duan)

Building energy consumption in China had increased by 40% from 1990 to 2009 as the incomes rise and urbanisation advances [1]. The energy consumed by space cooling accounts for around 10% of total building energy use in 2012 [2]. With global warming and rising demand for comfort levels, this share has been increasing continuously. Due to the participations of compressor and refrigerant, the dominant vapour compression refrigeration/air conditioning systems consume large amounts of electrical energy and cause heavy environmental impact. In comparison, Indirect Evaporative Cooling systems (IECs) utilise latent heat of water vaporisation to remove the heat from supply airflow and retain the moisture constant without using compressors and refrigerants that have great potentials in energy saving and associated carbon emissions reduction [3]. However, conventional IECs haven't been widely applied because the ultimate temperature for the IECs' supply air is the wet-bulb temperature of ambient air, which could hardly be achieved in practice. According to Ref. [4], it is thought that only 40 to 80 per cent of temperature difference between ambient air dry-bulb and wet-bulb could be reached in typical indirect evaporative coolers.

Regenerative or Recuperator Evaporative Cooler (REC), as the IECs with closed-loop configuration, has the ability of providing supply air at a temperature below the wet-bulb towards the dew-point temperature of inlet air theoretically [5-7]. According to the estimates [8], a counter-flow REC could annually reduce 13-58% of the total electrical power consumed by conventional compression air conditioners for various climates in China.

Predominantly, there are two types of regenerative evaporative coolers including single-stage counter-flow and multi-stage M-cycle cross-flow configurations [9]. Fig.1 demonstrates the working principles of their basic heat and mass exchanger structure and the psychrometric charts representing thermal process of airflows in dry and wet channels. In the counter-flow regenerative configuration, the intake airflow is circulated through the dry channel, a portion of the airflow is used as cooled product/supply airflow to be delivered to indoors, while being extracted through the perforations, the remaining airflow, as the working air, is re-circulated through the wet channel and is subsequently discarded to the outside. During this thermal process, the product air is cooled along the dry channel without any humidity increase whereas the working air is initially cooled to the minimal temperature with moisture additions at a certain distance from the entrance due to the effect of water evaporation. The temperature of working air subsequently begins to increase with minor moisture increase when the sensible heat transfer from product air in the dry channel exceeds the effect of evaporation cooling [10]. In the remainder of the wet channel, the working air has already reached saturation and has gradually heated under this condition. Eventually, the working air can be heated and humidified towards a temperature a bit higher than the wet-bulb of intake air before it's exhausted. This counter-flow recirculation arrangement allows the working air to be fully cooled before entering the wet channel, thus leading to increased temperature difference and heat transfer between the working and product airflows.

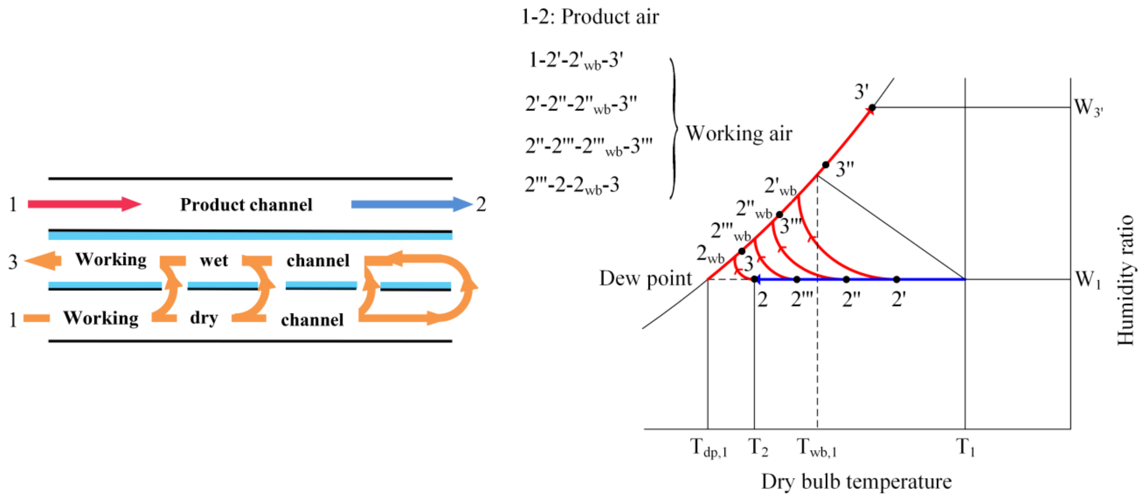

(a)

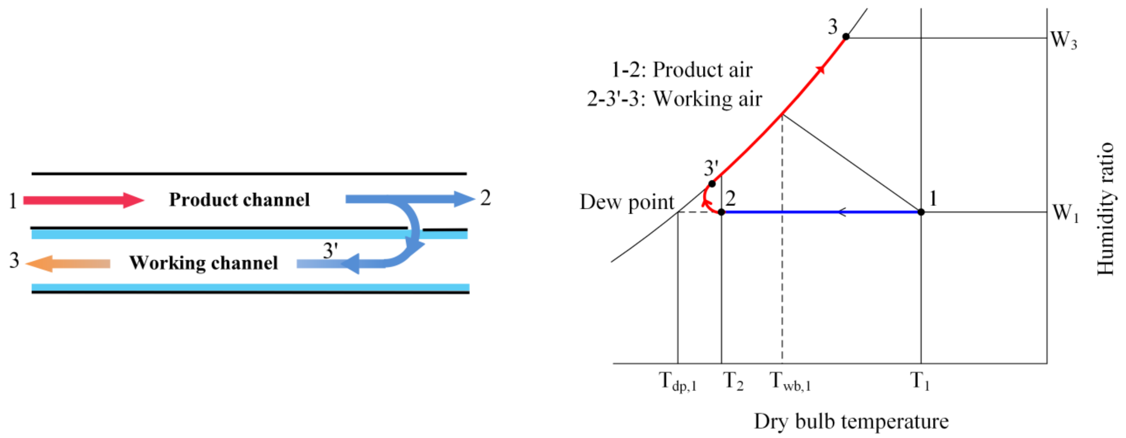

(b)

Fig. 1. Graphs showing working principle and psychrometric process of (a) M-cycle multi-stage regenerative HMX [ref] (b) single-stage regenerative HMX.

In the M-cycle regenerative configuration, part of the dry surface is designed for the product airflow to pass through while the rest is allocated to the working airflow. Both the product and working air flows parallel along the dry channel. A few perforations are evenly distributed over the surface where the working air is contained. Through the small holes, all of the air passing along the working dry channel is gradually diverted to the wet surface, to be used as working air. This portion of airflow is pre-cooled before entering the wet channel by losing heat to the adjacent wet surface. The working air flowing over the wet surface absorbs heat from the product and working air on dry surface. During the thermal process, the product air temperature is reduced with constant moisture, while the working air is partially pre-cooled, humidified and heated in multi-stage process (1-2'-2'wb-3', 2'-2"-2"wb-3", 2"-2'''-2'''wb-3''', 2'''-2-2wb-3) and is finally exhausted to the outside. Compared to the single-stage counter-flow cooler with equivalent physical size and operating conditions, this cross-flow cooler allows the working air to be cooled in multi-stage, thereby leading to 15-23% lower cooling effectiveness and around 20% smaller cooling capacity but 10% higher energy efficiency theoretically [11].

More recently, there have been growing interests on developing the single stage counter-flow and M-cycle regenerative evaporative coolers by analytical, numerical and experimental/field-testing methods. The analytical models being developed are normally based on conventional ε-NTU method when proper alternations are made by redefining the potential gradients, transfer coefficient, heat capacity rate parameters and assuming a linear saturation temperature-enthalpy relation of air. Through making these adjustments, the established analytical models can be used to determine the optimal operating and geometrical parameters of RECs for design problems, as well as to predict or compare the performance of RECs with different airflow patterns including parallel-flow, counter-flow, cross-flow and regenerative flow [10, 12-14]. Usually the analytical models were simplified to achieve acceptable results by making some assumptions, such as: 1) longitudinal thermal conduction in the wall is negligible; 2) Lewis number is unity, 3) heat and mass transfer coefficients inside each channel are constants; 4) water film is uniform and continuous, etc. [5, 13]. By contrast, some sophisticated models can provide more accurate predictions by considering a set of variables including Lewis factor, surface wettability, spray water temperature, and spray water enthalpy change [10, 12].

A few one-dimensional numerical models of counter-flow and two-dimensional models of M-cycle cross-flow RECs have been developed to predict/compare their performance and to analyse the effects of operating and geometrical parameters. The governing differential equations of these models were discretised with finite difference [15, 16] or finite element scheme [7, 11, 17] and solved using Newton iterative method or Eulerian-Lagrangian method [18]. The results of these modelling show that the RECs' performance strongly depends upon the parameters including intake air temperature and humidity, intake air velocity, working-to-intake airflow ratio, channel size of heat exchanger, feed water flow rate and uniformity of water film, but depends less on thermal conductivity of heat transfer sheets and feed water temperature [7, 19].

Additionally, a few experimental/fielding-testing studies have been conducted on counter-flow and M-cycle RECs aiming to 1) validate the numerical or analytical modelling results [16, 20], to 2) study the effects of operating parameters [16, 19, 21], to 3) achieve the internal air temperature and humidity distributions for dry and wet channels [22] and to 4) prove the cooler's technical viability through examining operating performance under various conditions [19, 23]. Most of those regenerative coolers developed are lab scale prototypes that can only provide sub-wet bulb cooling while operating at small intake channel air velocities lower than 1.0 m/s [16, 21]. As the intake air velocity increased from 1.0 to 4.0 m/s, the cooler's effectiveness dramatically declined by nearly 100% [18]. Therefore, to achieve desirable cooing effectiveness or outlet air temperature, the regenerative coolers are suggested to operate under the intake air velocity less than 1.0 m/s. In that case, the physical dimensions of the regenerative coolers have to be designed rather huge in order to deliver a large amount of supply airflow rate or cooling capacity. The question then arises: how to determine the geometric and operating parameters of the heat exchanger for accomplishing the REC optimal performance subject to specified design constraints such as certain cooling requirement and confined geometrical volume.

Aiming at solving the problem, this paper develops a computational model based on modified ε-NTU numerical method to determine the optimal geometrical and operating parameters of a new counter-flow regenerative evaporative cooler designed for buildings. The technical viability of the proposed cooler is confirmed by constructing a dedicated experimental prototype and testing it under various operating conditions in an air-conditioned chamber. The overall performance of the prototype examined in this study includes cooling effectiveness, cooling capacity, and energy efficiency as well as supply air temperature. The cooler's unit performance indicators include cooling capacity per unit volume and per airflow rate. Additionally, the paper experimentally and numerically analyses and compares the factors that affecting the cooler's overall performance, including intake air temperature, humidity, airflow rate and working-to-intake air ratio. To reveal the superior performance of the proposed cooler, the paper finally makes comparisons with those regenerative cooler found in previous studies in terms of overall/unit performance indicators under similar operating conditions.

2. Description of the developed counter-flow regenerative evaporative cooler

As depicted in Fig. 2, the regenerative evaporative cooler developed in this study is a self-contained device, mainly composed of a core heat and mass exchanger, a centrifugal fan, a water distributing/recirculating system and an outer casing. Ambient air is drawn into the cooler by the centrifugal fan, and is primarily filtered before entering the heat exchanger. In the exchanger where the thermal process going through by the process air is equivalent to that shown on the psychrometric charts in Fig. 1(b): The process air consisting of product and working air is cooled along the dry channels without moisture increase and subsequently discharged from the right side. Through the perforations located on the end of channels, a portion of the process air (as the working air) is diverted into the adjacent wet channels. Flowing in counter direction to the process air in dry channels, the working air of wet channels is humidified, heated and finally exhausted to outside. Meanwhile the remainder of process air (as the product air) is purified by a filtration again before it is supplied to outside. A damper was equipped to regulate the ratio of working to product airflow rate. A top water distributor enables water spread evenly across the wet surfaces of heat exchanger. Non-evaporated water is collected in the bottom reservoir and re-circulated to the top reservoir periodically through an electrical pump. When a certain amount of water is consumed, more fresh water is supplied to the top reservoir with a solenoid valve.

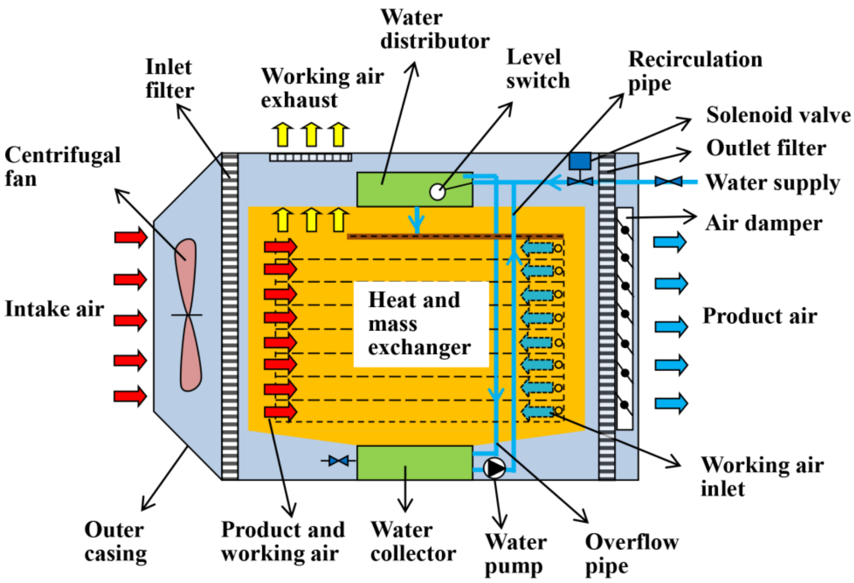

Fig. 2. Schematic diagram of the counter-flow regenerative evaporative cooler

3. Theoretical design of heat and mass exchanger

3.1. Overall and unit performance indicators

Wet-bulb effectiveness of the regenerative cooler, given by Eq. (1), is defined as the ratio of temperature reduction of inlet and outlet air dry-bulb to that of inlet air dry-bulb and wet-bulb.

$$\varepsilon_{wb} = \frac{t_{h,in} - t_{h,out}}{t_{h,in} - t_{h,in,wb}} \tag{1}$$

The cooler's sensible cooling capacity is determined by Eq. (2) derived from ASHRAE Standard 143 [24], when outside ambient air is used as the inlet air.

$$Q_{cooling} = \frac{c_{p,a}\rho_a (V_h - V_c)(t_{h,in} - t_{h,out})}{3.6} \tag{2}$$

Energy Efficiency Ratio (EER) of the evaporative cooler, calculated by Eq. (3), is described as the ratio of sensible cooling capacity to total power consumption of the cooler, i.e. electricity consumption by the air fan and water pump.

$$EER = \frac{Q_{cooling}}{P_{total}} \tag{3}$$

The cooler's unit performance indicators includes cooling capacity per unit volume and per unit airflow rate, which are the sensible cooling capacity determined by Eq. (2) divided by the cooler's geometric volume and supply airflow rate respectively.

3.2. Descriptions of the design problem

The design problem of heat and mass exchanger is complex that involves our comprehensive concerns on the exchanger's intended purpose, geometrical dimensions, capital investment and operating cost. In this study, the following design criteria were considered as a guideline:

- High cooling effectiveness (counter-flow pattern)
- Low pressure drop of airflows, i.e. low fan power consumption
- Compact size of exchanger, i.e. the exchanger's total length and depth are limited within 0.9 and 1.1 m respectively.
- Simple production and construction

To satisfy these needs, we designed a compact counter-flow plate-type heat and mass exchanger. The schematic of the exchanger is shown in Fig. 3. The exchanger comprises a stack of thin cellulose fibre coated plastic sheets, separated by N_{ch} channel gaps. The width (b) and depth (e) of each dry/wet channel gap is set to 3.0 mm and 45.8 mm (>15 times the width) respectively to achieve better heat transfer. The total width of effective heat transfer surface (W) is 0.458 m regardless of the supporting rods between the channels. The thickness of heat exchanger sheets (δ) is 0.375 mm. Therefore, the total depth of exchanger is $H=bN_{ch}+(N_{ch}+1)\delta$. The intake air design temperature is set to $t_{h,in}$ =37.78 ^{o}C dry bulb and $t_{h,in,wb}$=21.11 ^{o}C wet bulb (Australian standard rating condition, see Ref. [25]). The exchanger is required to provide $Q_{cooling}$=8303 W of cooling capacity with 1530 m^3/h supply/product airflow volumetric rate (V_h-V_c). It's able to supply sufficient air change rate by 1530 m^3/h due to 100% fresh air input, which totally fulfils the demands of the UK's building code [26] (the necessary air change rate for most types of buildings ranges from 4 to 10 ach for 100 m^2 floor area, which is equivalent to 400-1000 m^3/h approximately). Calculated by Eqs. (1) and (2) respectively, the exchanger's wet bulb effectiveness (ε_{wb}) and product air temperature were yield, i.e. ε_{wb}=0.977, $t_{h,out}$=21.5 ^{o}C, which are the known parameters for this design problem.

To meet the aforementioned design criteria, the exchanger's optimal geometrical and operating parameters should be determined that incorporate dry/wet channel length and depth (L, H), dry and wet channel numbers (N_{ch}), working-to-intake airflow ratio (R) and intake air velocity or intake airflow volumetric rate (V_h). A numerical computer model based on modified ε-NTU method is developed as follows to accomplish the purpose.

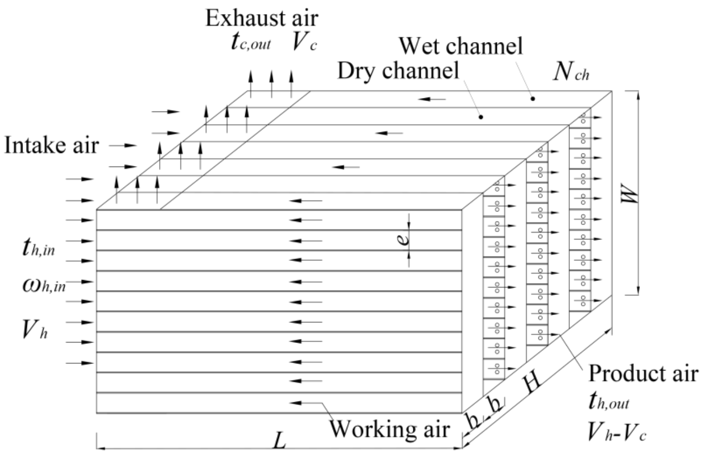

Fig. 3. Schematic of the counter-flow plate-type heat and mass exchanger

3.3. Modified effectiveness-NTU method

3.3.1. Mathematical equations and computational modelling method

The method applied for obtaining a numerical solution to the counter-flow heat and mass exchanger problem is to divide the entire heat exchanger into N numbers of computational elements. Fig. 4 illustrates the diagrams of computational element for the numerical modelling with the modified thermal profiles of the entire heat exchanger. A one-dimensional numerical model is developed by applying the modified ε-NTU method to each element of the exchanger and requiring that the boundary conditions associated with each element are consistent with the adjacent element. The numerical problem is coded in Engineering Equation Solver (EES) software and solved by Newton's alternative method. Some assumptions are made to simplify the solutions: 1) the exchanger is assumed to be well insulated to the surrounding; 2) longitudinal thermal conduction in the wall sheet is neglected; 3) fouling resistance of the exchanger is neglected; 4) heat and mass transfer coefficients as well as fluid properties inside each element of the model are constants; 5) Reynolds analogy between heat and mass transfer is valid and the Lewis number is unity; 6) the air-water interface offers a negligible resistance to heat transfer so that the interface temperature is saturated at the water film temperature.

In the modified ε-NTU method, the differential governing equations are directly given below regardless of the mathematical derivation, as the related study is well presented in Ref. [13]. In those equations, proper adjustment is made by redefining some terms stated in typical ε-NTU method, which include: 1) the enthalpy potential gradient for driving the energy transfer between the product air in dry channel and working air in wet channel; 2) the overall heat transfer coefficient and 3) the heat capacity rate parameters.

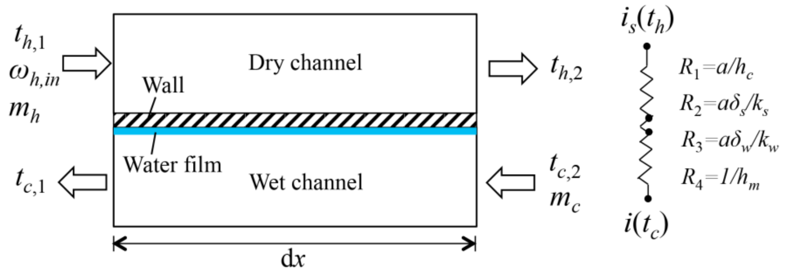

(a)

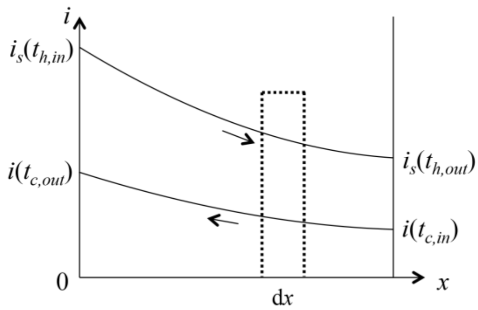

(b)

Fig. 4. Schematic diagrams illustrating (a) computational element for the numerical modelling and (b) modified thermal profiles of the counter-flow heat and mass exchanger

Based on the energy balance on the product air in dry side, the heat transfer rate for each computational element of the exchanger is given by Eq. (4):

$$dq = m_h(i_{h,1} - i_{h,2}) \tag{4}$$

where $i_{h,1}$ and $i_{h,2}$ represent the specific enthalpy of the process/primary air at the inlet and outlet states of each element respectively. An energy balance on the working air in wet side for each element is expressed as Eq. (5):

$$dq = m_c(i_{c,1} - i_{c,2}) \tag{5}$$

where $i_{c,1}$ and $i_{c,2}$ denote the specific enthalpy of the working air at the outlet and inlet states of each element respectively. For the regenerative cooler, the outlet thermal condition of the air in dry channel is equal to the inlet thermal condition of air in wet channel i.e. $i_{h,out} = i_{c,in}$ and $t_{h,out} = t_{c,in}$.

The heat transfer equation between the product air in the dry channel and the working air in the wet channel for the element can be given by Eq. (6):

$$dq = UdA\left(i_s(t_h) - i(t_c)\right) \tag{6}$$

Where the unique enthalpy gradient $i_s(t_h)$-$i(t_c)$ is the driven force making this energy transfer occur. The overall conductance of the heat exchanger is expressed in Eq. (7):

$$UdA = \left(a\left(\frac{1}{h_c} + \frac{\delta}{k} + \frac{\delta_w}{k_w} \right) + \frac{1}{h_m\sigma} \right)^{-1} N_{ch}Wdx \tag{7}$$

where σ is the surface wetting factor defined as the ratio of wetting area to the total area of heat transfer, which stands for surface incomplete wetting condition. It varies from 0 to 1 depending on surface wettability, water spraying condition and operating condition. In this study, a typical value of 0.8 was selected for this variable to carry out the modelling [12]. k and k_w symbolise the thermal conductivity of exchanger wall and water film. δ_w represents the thickness of water film, which was assumed to be 0.3 mm.

The enthalpy of air is assumed to have a linear relation with saturation temperature, which can be defined as Eq. (8).

$$i_s(t_h) = a(t_h) + c \tag{8}$$

Where a is the slope of the temperature-enthalpy saturation line and c is a constant in this equation.

The heat capacity rate of primary air (C_h) and secondary/working air (C_c) can be redefined by establishing the heat balance on the air in dry channel and wet channel, which are given in Eqs. (9) and (10) respectively:

$$m_h C_{p,h}(t_{h,1} - t_{h,2}) = C_h \left((i_s(t_{h,1}) - i_s(t_{h,2}) \right) \tag{9}$$

$$m_c C_{p,c}(t_{c,1} - t_{c,2}) = C_c \left(i(t_{c,1}) - i(t_{c,2}) \right) \tag{10}$$

Rearranging the Eq. (9) gives:

$$C_h = m_h C_{p,h} \frac{t_{h,1} - t_{h,2}}{i_s(t_{h,1}) - i_s(t_{h,2})} = \frac{m_h C_{p,h}}{a} \tag{11}$$

Where a can be determined by the ratio of enthalpy difference to the temperature difference between inlet and outlet air in each element of dry channel.

Rearranging the Eq. (10) gives:

$$C_c = m_c \frac{C_{p,c}(t_{c,1} - t_{c,2})}{i(t_{c,1}) - i(t_{c,2})} = m_c \tag{12}$$

The maximum possible heat transfer rate ($q_{\max}$) for the exchanger can be achieved theoretically as the overall conductance (UA) approaches infinity. The fluid with the minimum capacity rate ($C_{\min}$) will experience the maximum possible enthalpy gradient and the maximum heat transfer rate, which can be written as Eq. (13):

$$dq_{\max} = C_{\min} \left(i_s(t_h) - i(t_c) \right) \tag{13}$$

Where $C_{\min,i} = \min(C_h, C_c)$ (14)

The effectiveness of each computational element (ε) is the ratio of the actual heat transfer rate to the maximum possible heat transfer rate:

$$\varepsilon = \frac{dq}{dq_{\max}} \tag{15}$$

Substituting for $dq_{\max}$ from Eq. (13) into Eq. (15) yields:

$$\varepsilon = \frac{dq}{C_{\min} \left(i_s(t_h) - i(t_c) \right)} \tag{16}$$

The number of transfer units and the capacity ratio is expressed as Eqs. (17) and (18) respectively:

$$NTU = \frac{UdA}{C_{\min}} \tag{17}$$

$$C_r = \frac{C_{\min}}{C_{\max}} \tag{18}$$

Where $C_{\max} = \max(C_h, C_c)$ (19)

For a counter-flow exchanger, the effectiveness is determined by Eq. (20) [27]:

$$\varepsilon = \frac{1-\exp\left[-NTU(1-C_r)\right]}{1-C_r\exp\left[-NTU(1-C_r)\right]} \tag{20}$$

where C_r<1

3.3.2. Heat and mass transfer coefficients

In the Eq. (7), the convective heat transfer coefficient (h_c) of the product air in dry channel can be determined as follows. The air velocities in dry and wet channels are calculated by Eqs. (21) and (22) respectively:

$$u_h = \frac{V_h}{0.5WbN_{ch}} \tag{21}$$

$$u_c = \frac{V_c}{0.5WbN_{ch}} \tag{22}$$

Calculating the hydraulic diameter of dry and wet channels yields:

$$D_h = \frac{4\times b\times e}{2(b+e)} \tag{23}$$

For each computational element of heat exchanger, Reynolds number (*Re*) of the primary and secondary air in dry and wet channels is calculated by Eqs. (24) and (25) respectively:

$$Re_h = \frac{u_h D_h}{\nu_h} \tag{24}$$

$$Re_c = \frac{u_c D_h}{\nu_c} \tag{25}$$

Where ν_h and ν_c denote the kinematic viscosity of process and working air evaluated at average temperature in each element. The Reynolds numbers calculated by above equations are less than 2300, which indicates both the process and working airstreams are laminar flow.

The local convective heat transfer coefficients from process and working air to exchanger walls are decided by Eqs. (26) and (27) respectively:

$$h_{c,h}=\frac{Nu_{T,h}\cdot k_h}{D_h} \tag{26}$$

$$h_{c,c}=\frac{Nu_{T,c}\cdot k_c}{D_h} \tag{27}$$

where k_h and k_c respectively denote the thermal conductivity of process and working air evaluated at average temperature in each element. To obtain the conservative solution, $Nu_{T,h}$ represents the lower bound of local Nusselt number for a laminar, hydrodynamically and thermally fully developed flow in a rectangular duct that is exposed to an uniform wall temperature, which is given by Eq. (28) [28]

$$Nu_{T,fd}=7.541\left(1-2.610(b/e)+4.970(b/e)^2-5.119(b/e)^3+2.702(b/e)^4-0.548(b/e)^5\right) \tag{28}$$

where b/e=0.066 is defined by the aspect ratio of the minimum to the maximum dimensions of rectangular duct. While the local Nusslet number for a simultaneously developing flow in the rectangular duct as a function of dimensionless position, $L/(D_hRePr)$, was predicted by EES procedure, i.e. DuctFlow_N_local [29], which interpolated a table of data provided by Ref. [30]. Assuming that the Lewis number for air and water mixture is unity, the mass transfer coefficient between working air and water film can be obtained by the following equation:

$$h_m=\frac{h_{c,c}}{C_{p,c}} \tag{29}$$

Where $C_{p,c}$ is the specific heat capacity of moist air assessed at average temperature of working air in each element.

3.3.3. Pressure drop of airflows

The total pressure drop of the process and working air, consisting of friction and minor loss, can be described in Eqs. (30) and (31) respectively.

$$\Delta p_{\text{total},h}=\int_0^L \Delta p_{f,h}+\sum \Delta p_{m,h} \tag{30}$$

$$\Delta p_{\text{total},c}=\int_0^L \Delta p_{f,c}+\sum \Delta p_{m,c} \tag{31}$$

where the friction loss of product air ($\mathbf{\Delta}P_{f,h}$) and working air ($\mathbf{\Delta}P_{f,c}$) in each element are calculated using the Eqs. (32) and (33) respectively [27]:

$$\Delta p_{f,h}=f_h\frac{\rho_h u^2{}_h}{2D_h}dx \tag{32}$$

$$\Delta p_{f,c} = f_c \frac{\rho_c u_c^2}{2D_h} dx \tag{33}$$

where the average friction factor (f) of each modelling element is computed by the empirical correlations expressed as Eq.(34) [28], for laminar flow in rectangular duct including the simultaneously developing and fully developed regions.

$$f \approx \frac{4}{\mathrm{Re}}\left[\frac{3.44}{\sqrt{L^+}} + \frac{\frac{1.25}{4L^+} + \frac{f_{fd}\,\mathrm{Re}}{4} - \frac{3.44}{\sqrt{L^+}}}{1 + \frac{0.00021}{\left(L^+\right)^2}}\right] \tag{34}$$

where $L^+=L/(D_h\mathrm{Re})$ is the dimensionless length for a hydro dynamically developing internal flow. The friction factor (f_{fd}) for the fully developed laminar flow in rectangular duct can be determined by the correlation given in Eq. (35) [28]:

$$f_{fd}\,\mathrm{Re} = 96(1 - 1.3553AR + 1.9467AR^2 - 1.7012AR^3 + 0.9564AR^4 - 0.2537AR^5) \tag{35}$$

The minor loss of product and working air in Eqs. (30) and (31) are calculated by Eqs. (36) and (37) respectively:

$$\sum \Delta p_{m,h} = \sum \zeta_h \frac{\rho_h u_h^2}{2} = (\zeta_{in,h} + \zeta_{\mathrm{tee,straight}} + \zeta_{filter})\frac{\rho_h u_h^2}{2} \tag{36}$$

$$\sum \Delta p_{m,c} = \sum \zeta_c \frac{\rho_c u_c^2}{2} = (\zeta_{\mathrm{tee,branched}} + \zeta_{\mathrm{contraction}} + \zeta_{\mathrm{expansion}} + \zeta_{\mathrm{bend}} + \zeta_{\mathrm{exit}})\frac{\rho_c u_c^2}{2} \tag{37}$$

where $\Sigma\zeta_h$ and $\Sigma\zeta_c$ denote the total minor loss coefficients of the product and working airflow in dry and wet side respectively. $\zeta_{in,h}$ and ζ_{exit} indicate the resistance coefficients for a sharped edged duct inlet and exit respectively. $\zeta_{\mathrm{tee,straight}}$ and $\zeta_{\mathrm{tee,branched}}$ are the resistance coefficients for standard T with flow straight through and primarily through branch respectively. $\zeta_{\mathrm{contraction}}$ and $\zeta_{\mathrm{expansion}}$ represent the resistance coefficients for an abrupt contraction and expansion processes respectively. ζ_{filter} and ζ_{bend} symbolise the resistance coefficients for an air filter and a 90 degree bend.

The actual fan power consumption is the ratio of the total theoretical energy use to the fan efficiency (η), which is given by Eq. (38):

$$P = \frac{\Delta p_{\mathrm{total},h} \cdot V_h + (\zeta_{\mathrm{exit}} + \zeta_{filter})\frac{\rho_h u_{h,out}^2}{2} \cdot (V_h - V_c) + \Delta p_{\mathrm{total},c} \cdot V_c}{\eta} \tag{38}$$

where $u_{h,out} = (V_h - V_c)/(0.5WbN_{ch})$, which is the outlet air velocity in dry channel.

3.4. Results and discussion of numerical modelling

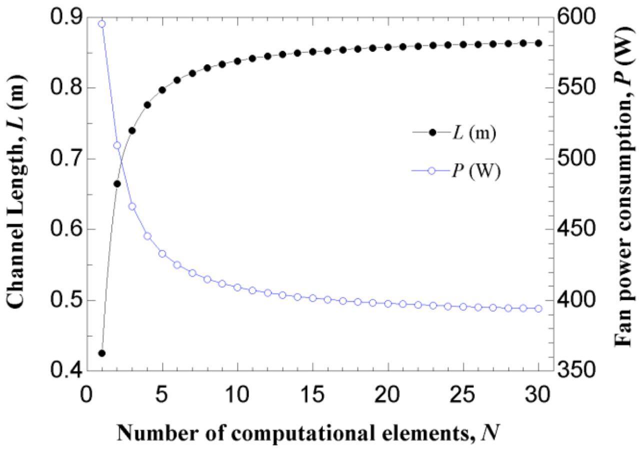

Fig. 5. Channel length and fan power consumption as a function of the number of computational elements

Fig. 5 plots the channel length predicted by the numerical model as a function of the number of computational elements. The result shows that the accurate results of channel length and power consumption can be achieved if the number of computational elements is larger than 20, which are 0.86 m and 394 W respectively.

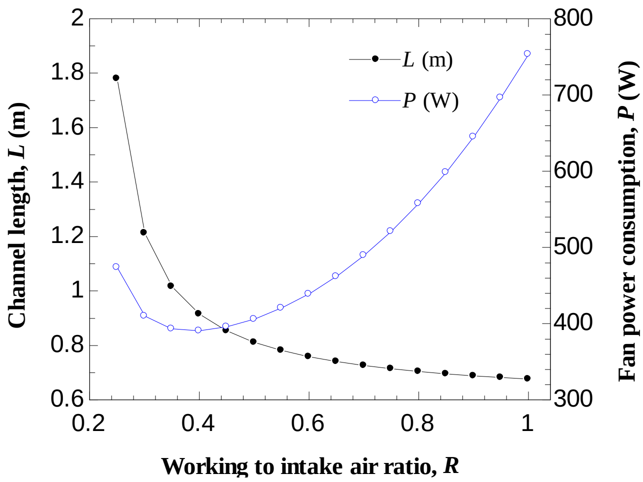

Fig. 6. Channel length and fan power consumption as a function of working-to-intake air ratio

Fig. 6 shows the effects of the ratio of working to intake airflow rate on channel length and fan power consumption. The predicted power consumption reaches minimum with the working-to-intake air ratio varied between 0.35 and 0.45. Also, the predicted channel length drops rapidly with the working-to-intake air ratio smaller than 0.44 and then it gradually decreases without changing too much. Therefore, to reduce the exchanger's capital and operating costs, its working-to-intake air ratio should be set around 0.44.

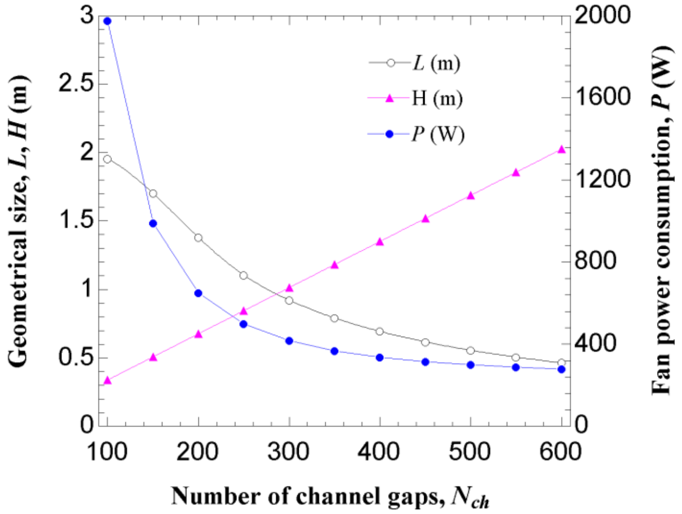

(a)

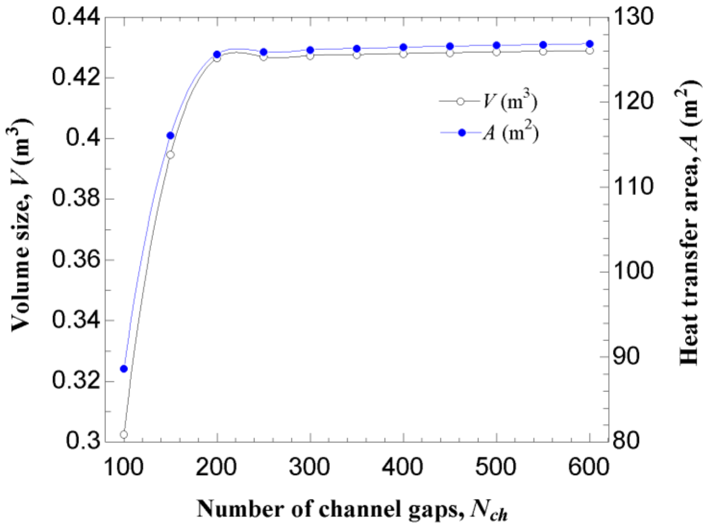

(b)

Fig. 7. Effects of number of channel gaps on (a) channel length, depth and fan power consumption; (b) volume size and heat transfer area of heat exchanger

Fig. 7 indicates the geometrical parameters (channel length and depth) and fan power consumption of the heat exchanger as a function of channel gaps number. With increasing the channel gap number from 100 to 600, the predicted channel length decreases from 1.96 to 0.46 m and the channel depth increases from 0.34 to 2.02 m. Meanwhile, It is shown that the prediction of fan power consumption reduces dramatically with the channel number increasing from 100 to 300 and nearly keeping constant from 300 to 600. The calculated volume size and heat transfer area of the exchanger doesn't vary too much while the channel number increasing from 200 to 600. All in all, the number of 320 channel gaps was determined by comprehensively considering design criteria including simple manufacturing, low energy consumption and limited geometry. The total depth of exchanger is 1.08 m derived from the number of channel gaps. In summary, Table 1 presents the geometrical and operating parameters of the heat exchanger, including the known design conditions and predicted results.

Table 1. Known and predicted design parameters of heat and mass exchanger

Design parameter	Symbol	Unit	Value
Intake air dry-bulb temperature	$t_{h,in}$	^{o}C	37.78
Intake air wet-bulb temperature	$t_{h,in,wb}$	^{o}C	21.11
Intake air humidity ratio	ω	g/kg	9.05
Product air volumetric flow rate	V_{h}-V_{c}	m^3/h	1530
Intake air volumetric flow rate	V_h	m^3/h	2737
Cooling capacity	$Q_{cooling}$	W	8303
Fan power consumption	P	W	394
Product air dry-bulb temperature	$t_{h,out}$	^{o}C	21.5
Wet-bulb effectiveness	ε_{wb}	-	0.977
Thickness of thin sheets	δ	mm	0.375
Thickness of water film	δ_w	mm	0.3
Dry/wet channel height	b	mm	3.0
Dry/wet channel width	e	mm	45.8
Dry/wet channel length	L	m	0.86
Total width of heat transfer surface	W	m	0.458
Total depth of the exchanger	H	m	1.08
Thermal conductivity of wall sheet	k	W/(m·K)	0.375
Thermal conductivity of water film	k_w	W/(m·K)	0.3
Fan efficiency	η		0.65
Working-to-intake air ratio	R	-	0.44
Number of dry and wet channels	N_{ch}	-	320

Figs. 8 and 9 respectively depict the effects of channel length and intake airflow rate on overall performance of the cooler while retaining other geometrical and operating parameters the same as shown in Table 1. They indicate that the model developed here can be used to determine the heat exchange's channel length and intake airflow rate if the required cooling effectiveness, cooling capacity and power consumption are known in advance.

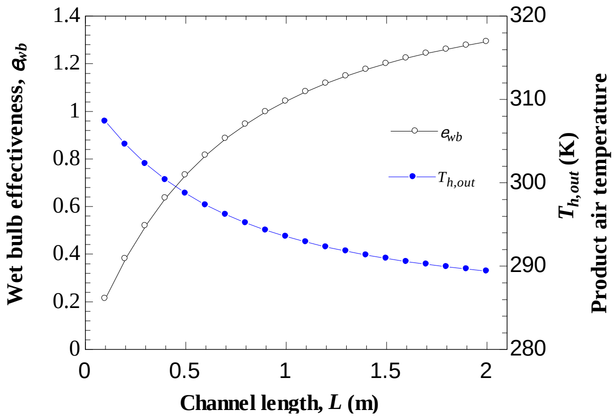

Fig. 8. Calculated wet bulb effectiveness and product air temperature as a function of channel length

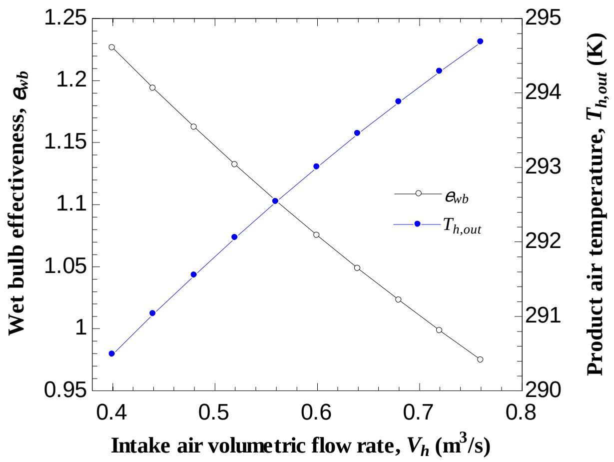

(a)

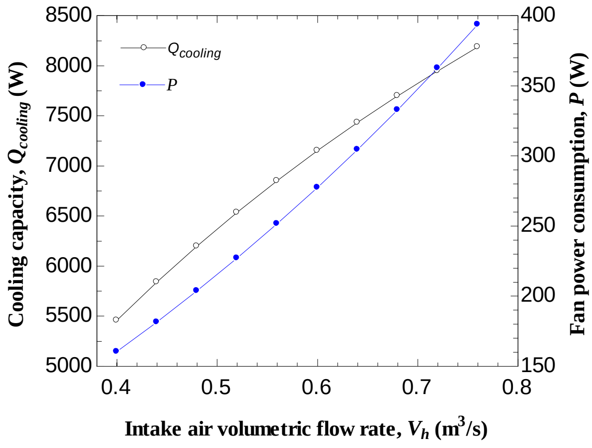

(b)

Fig. 9. Effects of intake air flow rate on (a) wet-bulb effectiveness and product air temperature; (b) cooling capacity and fan power consumption

4. Fabrication of the regenerative evaporative cooler

4.1. Heat and mass exchanger

The heat and mass exchanger was designed, fabricated and constructed as specifications summarised in Table 1. As seen in Fig. 10, the exchanger was stacked together using 160 pairs of dry and wet channels. The dry and wet channels were formed with moisture impervious polymer films and cellulose-blended wicking fibre films, which has superior water absorption and retention abilities compared to other hydrophilic materials [8]. Each dry or wet channel is separated by 10 pieces of long plastic rods having the dimensions of 2×3×860 mm and 2×3×695 mm respectively. These rods were arranged in parallel rows to form long paths with rectangular cross-section (3×45.8 mm), which are designed to guide the passing product and working airflows. Moreover, both two sides of the rods in between wet channels were coated with the same wicking fibre in order to enhance surface wetting condition. Aluminium strips (in 3×10×665 mm) coated with the same wicking fibre material were also constructed at the top of each wet channel to facilitate surface water distribution. It is found that the evaporation surfaces were completely wetted within 5 minutes with assistance of the strips.

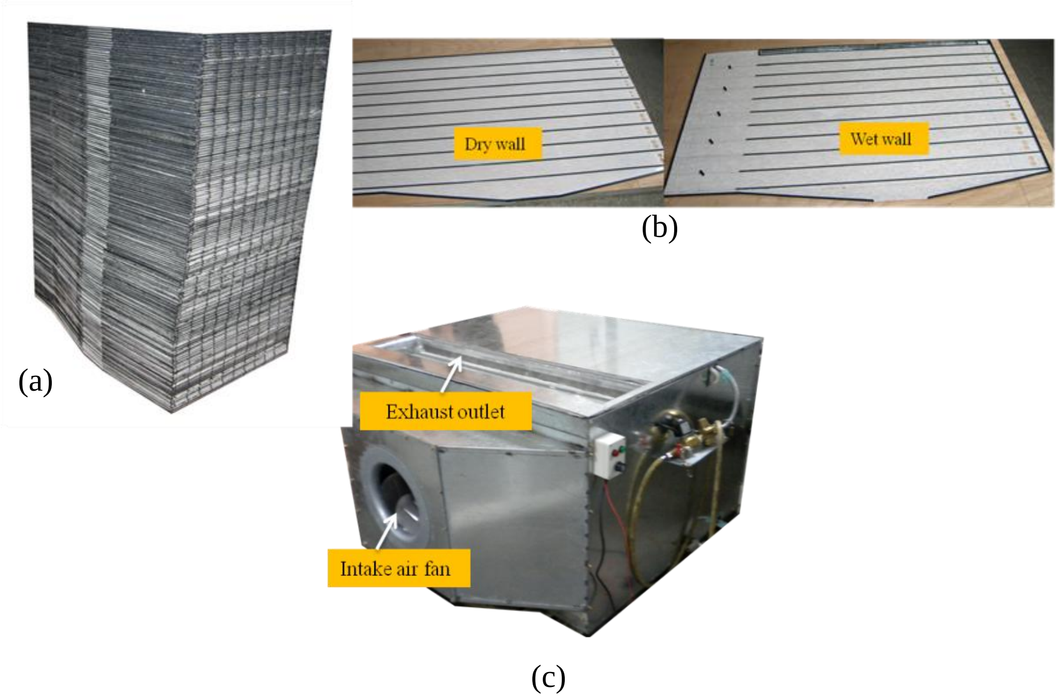

Fig. 10. Photographs showing the fabricated (a) exchanger, (b) dry/wet wall and (c) regenerative evaporative cooler

4.2. Regenerative evaporative cooler

The prototype of regenerative evaporative cooler was mainly assembled using the heat and mass exchanger, a centrifugal fan (manufacturer: ebm-papst, type: K3G355-AI62-06), a water distributor and collector as depicted in Fig. 2. A high efficiency filter made of fibrous materials, being installed between the fan and the inlet of exchanger, is used to remove solid particulates (such as dust, mould and bacteria) from process air and to make the intake air of exchanger distribute more uniformly. Another filter placing at the outlet of heat exchanger, not only to further purify the product air but also to block and divert portions of process air into the adjacent wet channels through the terminal perforations. Evaporation water is supplied from the top water distributor to the top of wet channels through 160 pieces of copper tubes in 2.6 mm outer diameter, located at internals of 6 mm, which is the distance between adjacent wet channels. Unused water is collected in bottom reservoir and recirculated to the top water distributor through an electrical pump (manufacturer: Xin Wei Cheng tech., type: WKA1300-12V). When the water level in the top distributor falls below the lower limit, a water level switch (manufacturer: Cynergy3, type: SSF211X100) can detect the level change and open a joint solenoid valve (manufacturer: COVNA, type: 2W31-15GBN). As a consequence, more fresh water will be supplied to the distributor until the upper limit is reached. The capital cost of the cooling unit was calculated by summing up the prices of the components contained in the unit, taking into account an appropriate rate of labour cost in China. It should be stressed that the prices of the components were quoted from the selected product catalogue and the labour cost was estimated on the basis of mass production premise. Details of the calculation are presented in Table 2.

Table 2. Estimated capital cost of the cooling unit

Component	Unit Price (CNY)	Quantity	Cost (CNY)
Centrifugal fan	10994	1 [piece]	10994
Electrical pump	495	1 [piece]	495
Air filter	100	2[piece]	200
Water distributor	100	1[piece]	100
Water collector	50	1[piece]	50
Solenoid valve	95	1[piece]	95
Supply air damper	80	1[piece]	80
Level switch	570	1[piece]	570
Outer casing	330	1[piece]	330
Heat exchanger	3700	1[piece]	3700
Labour cost	20	80[hours]	1600
Total			18214

5. Experimental set-up

5.1. Experimental instrumentation and measurement method

Fig. 11 demonstrates a layout of the experimental facility for testing the fabricated regenerative evaporative cooler's performance. The cooler was placed in an environmentally controlled room, which is conditioned by an Air Handling Unit (AHU) consisting of a pre-heater, a humidifier, a cooling coil, a re-heater and an air blower. The AHU was adjusted to vary the temperature and humidity of the entering air to the cooler. Both the supply and exhaust airflows of the evaporative cooler were connected to the separate airflow measurement chambers, which are composed of square tunnels with several flow nozzles in the middle. The supply or exhaust airflow rate given in Eq. (39), is obtained by measuring the difference in pressure across the taps at upstream and downstream of the nozzle plate using micro manometers (measurement range：0-1500 Pa, accuracy：0.01 mmH_2O).

$$q_v = CA\sqrt{\frac{2}{\rho}\left(P_1 - P_2\right)} \tag{39}$$

Where, q_v symbolises volumetric flow rate, m^3/s; C denotes orifice flow coefficient, i.e. 0.6, A is the cross-sectional area of the orifice hole, m^2; ρ is the air density, kg/m^3; P_1 and P_2 represent air pressures measured at upstream and downstream of the orifice plate respectively, Pa.

A variable-speed fan located at the outlet of each airflow chambers is used to maintain the required outlet static pressure and compensate for the additional resistance of the pipework and measurement system. The cooler's intake air flow rate was varied by the inlet fan, while its dry-bulb and wet-bulb temperatures were measured by dry-bulb and wet-bulb mercury thermometers (measurement range: -25-50 ^oC, accuracy:±0.2 ^oC) respectively, placed at the inlet of the air cooler. Small portions of the supply airflow were drawn by a blower to a visualised plastic box, where mercury thermometers (measurement range： 0-50 ^oC, accuracy：±0.1 ^oC) were positioned to measure its dry-bulb and wet-bulb temperature. Meanwhile, the cooler's exhaust air dry-bulb and wet-bulb temperatures were tested using the same method. The cooler's energy consumption was gauged using a power meter (measurement range: 0-1000 W, accuracy: ±0.01 W).

The measured data were analysed under steady states, which was defined as the period when the dry-bulb and wet-bulb temperature variations are within 0.1 ^oC for 10 minutes. Once steady state had been achieved, the dry-bulb, wet-bulb temperatures and pressures used for performance analysis were attained by taking algebraic average of the measured data over 10-minute intervals. The data collected enabled a number of performance indicators to be determined including wet-bulb effectiveness, cooling capacity, power consumption and EER.

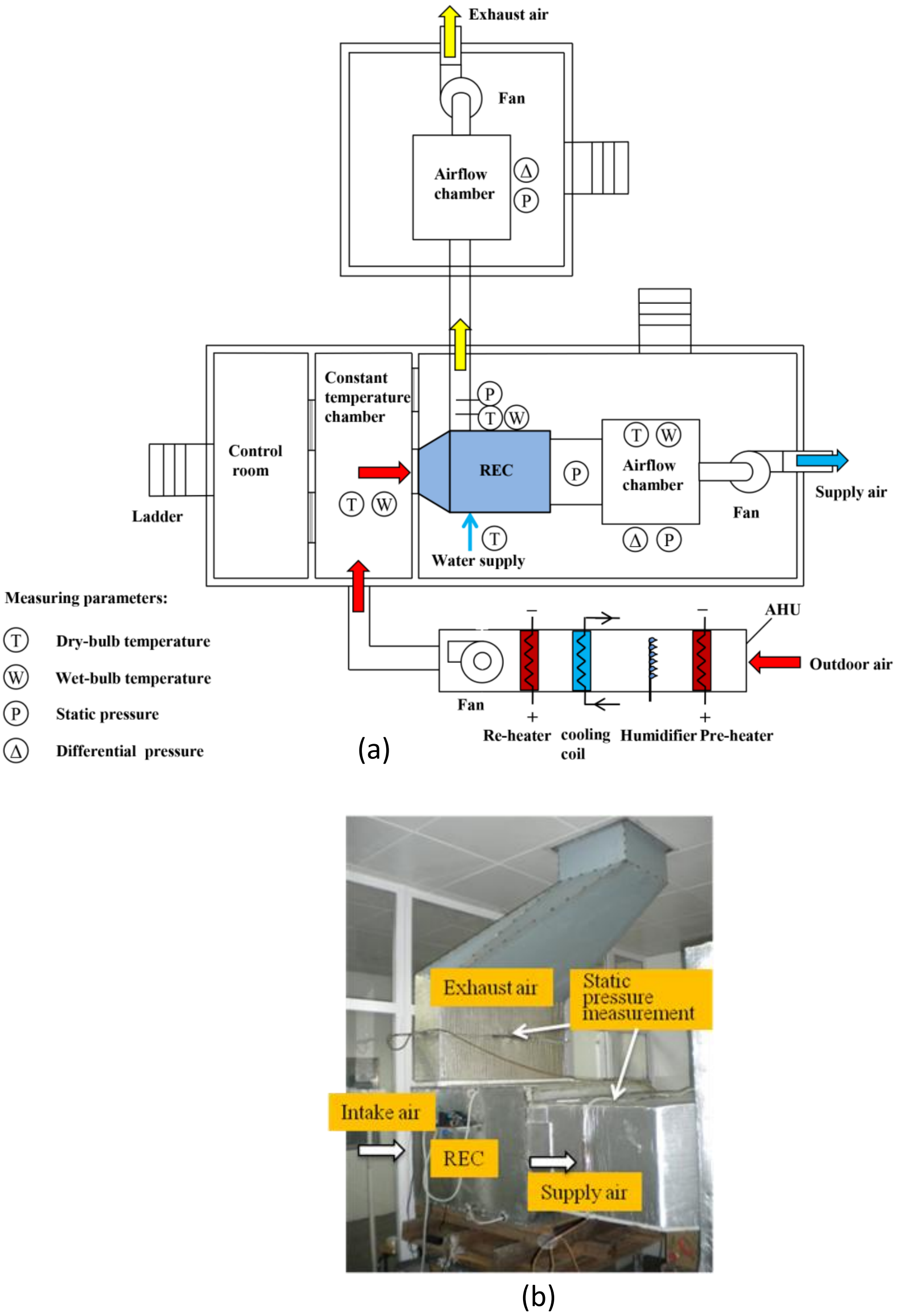

Fig. 11. Graphs showing (a) schematic and (b) photograph of the evaporative cooling system experimental set-up

5.2. Uncertainty analysis of experimental results

The accuracy of experimental results was examined by evaluating energy balance between the cooler's product air and the working air. The energy changes in product and working airflows are determined by Eqs. (40) and (41) respectively. Fig. 12 depicts the comparison of energy changes in product and working air for all experimental data conducted in this work. It is shown that, for most of cases, the energy changes agree well and the inconsistency is below ±10%.

$$E_p = m_1(h_1 - h_2) \tag{40}$$

$$E_w = m_3(h_3 - h_2) \tag{41}$$

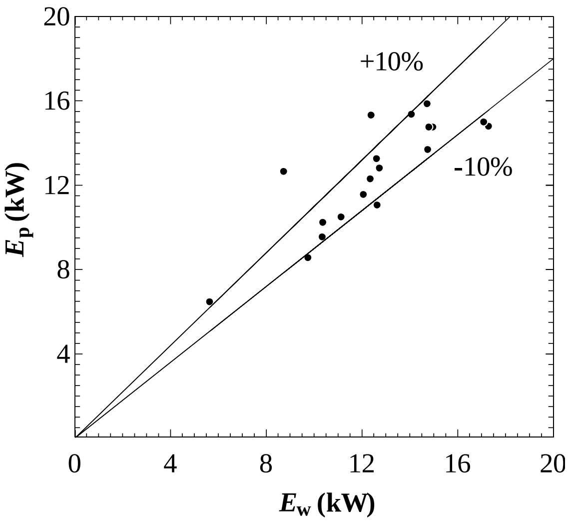

Fig. 12. Comparison between the energy changes in product and working airflows

Eq. (42) was given to calculate the relative uncertainty for the dependent performance indicator variables.

$$\frac{\Delta y}{y} = \sqrt{\sum_i \left(\frac{\partial y}{\partial x_i} \cdot \frac{\Delta x_i}{y}\right)^2} \tag{42}$$

Where $\Delta y/y$ represents the relative uncertainty of dependent variables, i.e. $\Delta\varepsilon_{wb}/\varepsilon_{wb}$, $\Delta Q_{cooling}/Q_{cooling}$, ΔEER/EER; y is the function of the independent variables x_i described in Eqs. (1)-(3) respectively. For instance, $y=\varepsilon_{wb}$, thus $x_i=t_{db,1}$, $t_{db,2}$, $t_{wb,1}$. The uncertainty of airflow rate is determined by pressure drop, given in Eq. (39). The uncertainty for the performance indicator variables was found to be within ±1.31% for wet-bulb effectiveness, ±1.36% for sensible cooling capacity and ±2.61% for EER on average.

6. Performance analysis of the regenerative evaporative cooler

The study experimentally examines the overall performance of the proposed regenerative cooling prototype under various operating conditions and compares the results with the predictions obtained from the aforementioned numerical work. It also analyses the factors that affecting its cooling performance including intake air temperature and humidity, intake airflow rate, and working-to-intake air ratio numerically and experimentally. The achieved results can be employed 1) to analyse the performance of the system in different operating conditions; 2) to optimise its overall performance by determining its appropriate operating parameters; 3) to confirm practicality of the counter-flow cooler applying in hot and dry climates and reveal its novelty characteristics through comparing with previous studies in terms of systems geometrical, operating and performance parameters.

6.1. Effect of intake airflow rate

Fig. 13 shows the cooler's cooling effectiveness, cooling capacity and EER value obtained from the experiment and simulation when gradually increasing the intake airflow rate from 1148 to 2393 m^3/h (corresponding to 1.73-3.60 m/s of intake channel air velocity) while keeping the other operating parameters constant ($t_{h,in}$=38.0 ^oC d.b., $t_{h,in,wb}$=20.8 ^oC w.b., t_w=22 ^oC and R=0.47). It is observed that, for the experimental data, as the intake airflow rate increased by 108%, the cooler's wet-bulb effectiveness declined merely by 7.6% from 1.07 to 0.99 while the supply air temperature increased by 6.6% from 19.6 to 20.9 ^oC. With the same change, the cooling capacity of the system was significantly increased from 3.9 to 7.3 kW by around 84% and the EER from 10.6 to 16.9 by 58.6%. The results show that, when operating under a wide range of intake air velocity (1.73-3.04 m/s), the established prototype could reduce the intake air temperature below its wet-bulb and provide much higher cooling capacity with only a small amount of energy consumption.

It is also found that the discrepancies between the numerical and experimental results ranged from 5.3-19.2%, 3.9-14.4% and 3.9-21.5% in terms of cooling effectiveness, cooling capacity and supply air temperature respectively. The differences are getting larger when intake airflow rate are reduced. For the lowest intake airflow rate, there was biggest gap occurred between the experimental and predicted data. The reason for the increased discrepancy can be explained as follows: For the experiment results, as the intake airflow rate is reduced, the water evaporation rate is getting slower as plotted in the Fig. 11(b) of Ref. [19]. Thus, the ratio of water supplied to water evaporated is getting higher while reducing the intake airflow rate because the water mass flow rate supplied to the exchanger is predominantly constant during the experiment process. The highest water supplied-to-evaporated ratio makes the cooler's effectiveness fall to the lowest level as indicated in the Fig. 6 of Ref. [20]. For the simulation results, however, the uniform and continuous water film is always assumed for all operating conditions without considering excessive water mass flow rate, which could become much larger in the experiment when the intake airflow rate is getting smaller. Therefore, the measured performance is substantially less than that predicted. This discrepancy may be reduced if the feed water mass flow rate was made small in the exchanger while keeping the evaporation surfaces completely wet. Especially, a smaller water mass flow rate should be supplied when the intake airflow rate is small. The similar trend of this discrepancy between measured and predicted effectiveness was also described in the Fig. 3 of an early paper [5], in which assuming that constant water mass flow rate was maintained while varying the air flow rates, the water flow rates would be most excessive and measurements lowest relative to the predictions at low Reynolds numbers, i.e. low air velocities.

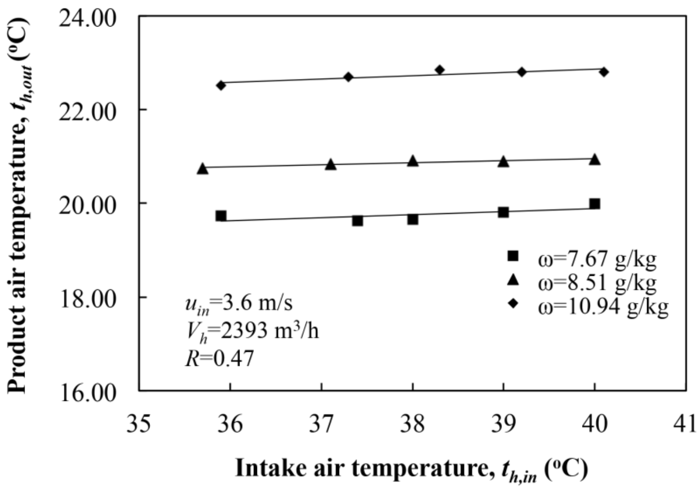

(a)

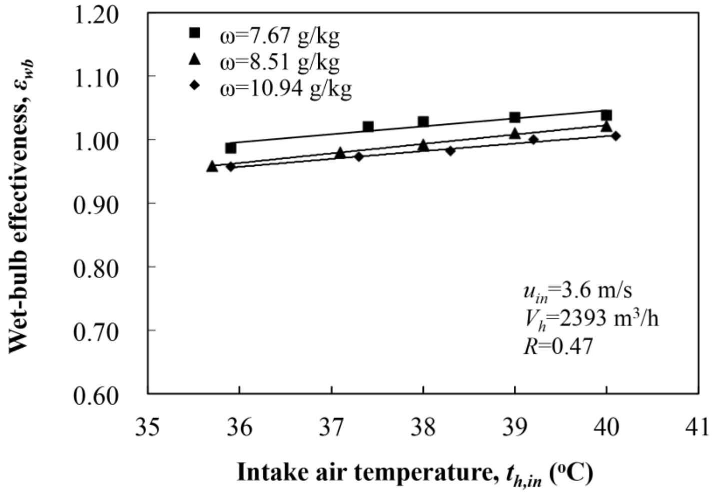

(b)

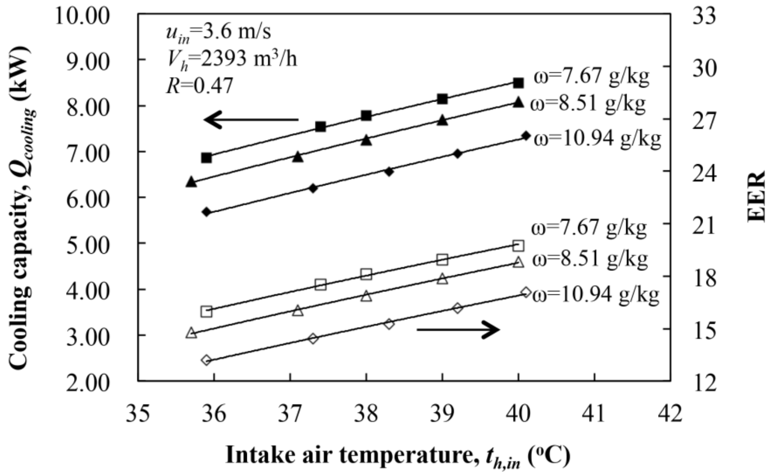

(c)

Fig. 13. Graphs showing the effect of intake airflow rate on the cooler's (a) product air temperature (b) wet-bulb effectiveness (c) cooling capacity and EER

6.2. Effect of intake air temperature and humidity

Fig. 14 depicts the cooler's overall performance evaluated experimentally and numerically under different intake air humidity ratio (ω=7.67, 8.51, 10.94 g/kg) when gradually increasing the intake air dry-bulb temperature from 36 to 40 ^{o}C while retaining the other operating parameters constant (u_{in}=3.6 m/s, V_h=2393 m^3/h, R=0.47, t_w=25.3 ^{o}C). It is found that the cooler's cooling capacity and effectiveness, together with the energy efficiency were linearly growing with increasing the intake air temperature. Operating at highest intake airflow rate, the cooler can achieve 0.96 to 1.04 of wet-bulb effectiveness approximately. The hot intake air can be cooled to 19.7-22.9 ^{o}C (around 1 ^{o}C lower than the wet-bulb temperature of intake air) before it was finally supplied to outside, bring about 13.4-20.0 ^{o}C of temperature reduction. These results indicate the cooling prototype can obtain sub-wet bulb supply air temperature even for the largest intake airflow rate, and it is greatly influenced by the intake air temperature and humidity with respect to the overall performance, as described in Eqs. (1) and (2).

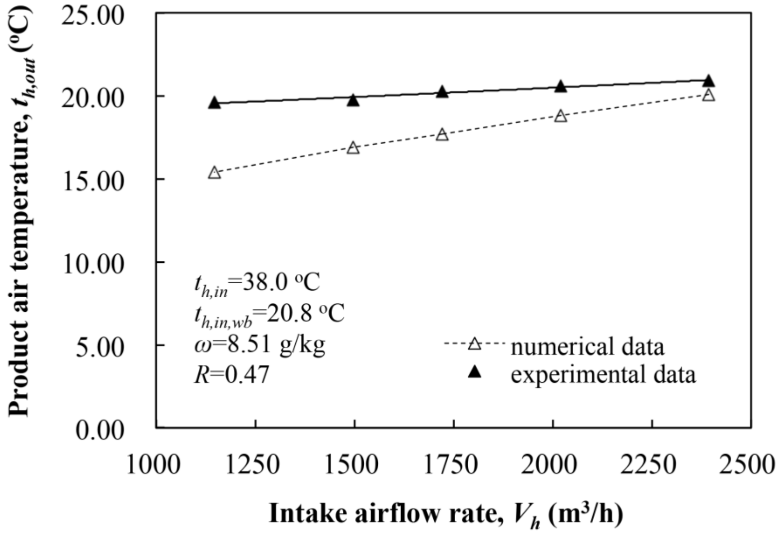

Product air temperature, $t_{h,out}$ (°C)
25.00
20.00
15.00
10.00
5.00
0.00
1000
1250
1500
1750
2000
2250
2500
Intake airflow rate, V_h (m³/h)
$t_{h,in}$=38.0 °C
$t_{h,in,wb}$=20.8 °C
ω=8.51 g/kg
R=0.47
numerical data
experimental data

(a)

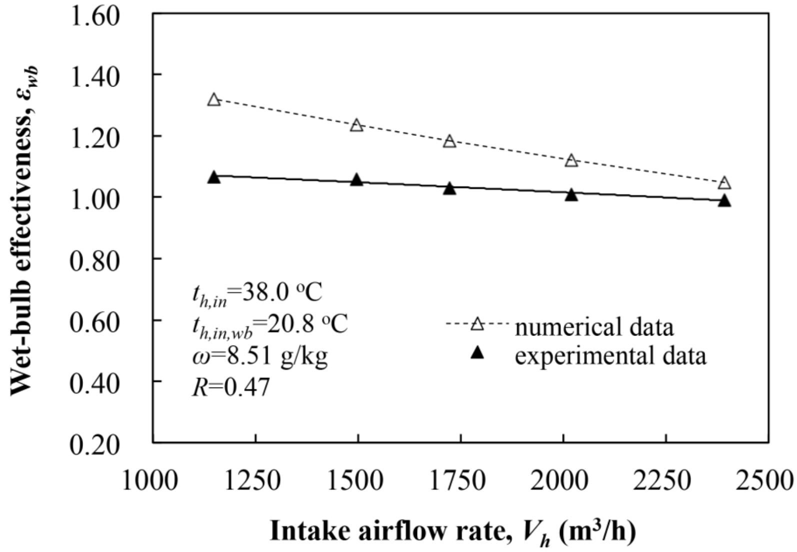

Wet-bulb effectiveness, ε_{wb}
1.60
1.40
1.20
1.00
0.80
0.60
0.40
0.20
1000
1250
1500
1750
2000
2250
2500
Intake airflow rate, V_h (m³/h)
$t_{h,in}$=38.0 °C
$t_{h,in,wb}$=20.8 °C
ω=8.51 g/kg
R=0.47
numerical data
experimental data

(b)

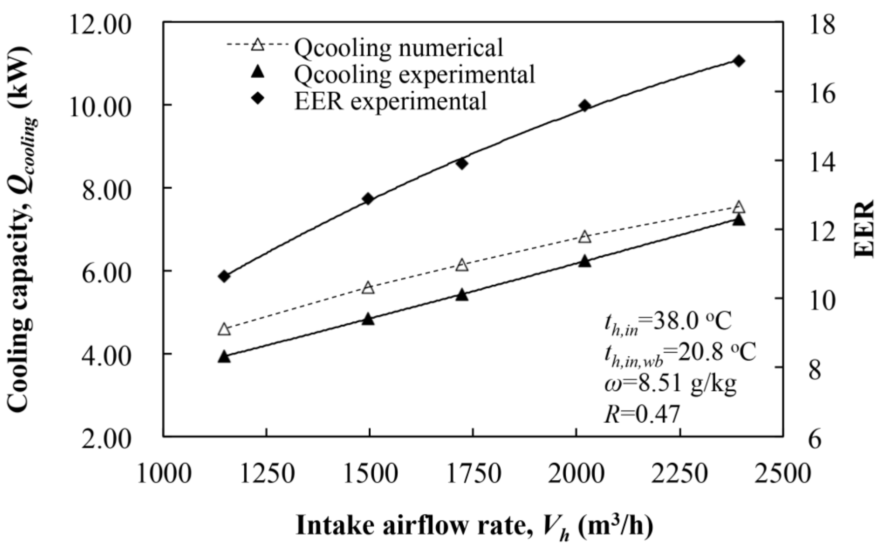

Cooling capacity, $Q_{cooling}$ (kW)
12.00
10.00
8.00
6.00
4.00
2.00
EER
18
16
14
12
10
8
6
1000
1250
1500
1750
2000
2250
2500
Intake airflow rate, V_h (m³/h)
Qcooling numerical
Qcooling experimental
EER experimental
$t_{h,in}$=38.0 °C
$t_{h,in,wb}$=20.8 °C
ω=8.51 g/kg
R=0.47

(c)

Fig. 14. Graphs showing the effect of intake air temperature and humidity on the cooler's (a) product air temperature (b) wet-bulb effectiveness (c) cooling capacity and EER

6.3. Effect of working-to-intake air ratio

Fig. 15 demonstrates the cooler's overall performance examined experimentally and numerically under different working-to-intake airflow rate ratio while keeping the other operating conditions fixed ($t_{h,in}$=38.9 °C, $t_{h,in,wb}$=21.2 °C, V_h=2393 m^3/h, R=0.47). The experimental results show that the working to intake air ratio evidently affects the cooler's overall performance. With the ratio getting higher, the cooler's wet-bulb effectiveness increased by 15.8% from 0.85 to 0.99 and the supply air temperature dropped by 8.4% from 23.7 to 21.7 °C. Meanwhile, the cooling capacity and EER value enhanced with the ratio increasing from 0.35 to 0.44 and then fell down from 0.44 to 0.58. Hence, considering the contrary variation trends among the wet-bulb effectiveness, cooling capacity and energy efficiency, the optimal ratio of working to intake airflow rate should be around 0.4-0.44.

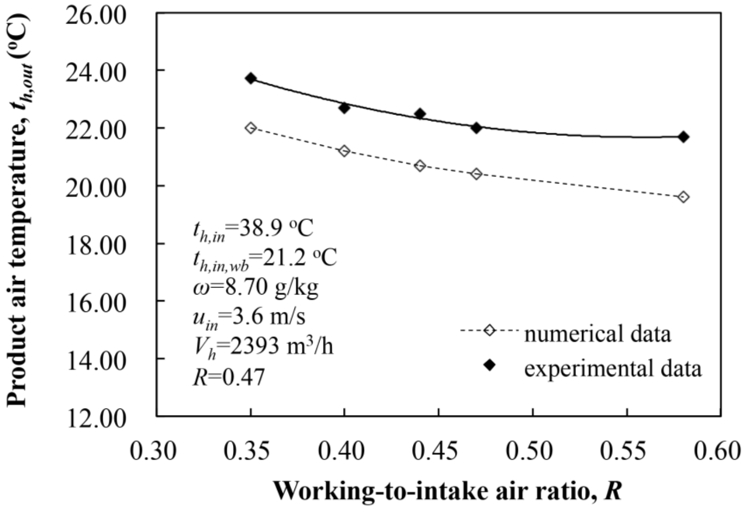

(a)

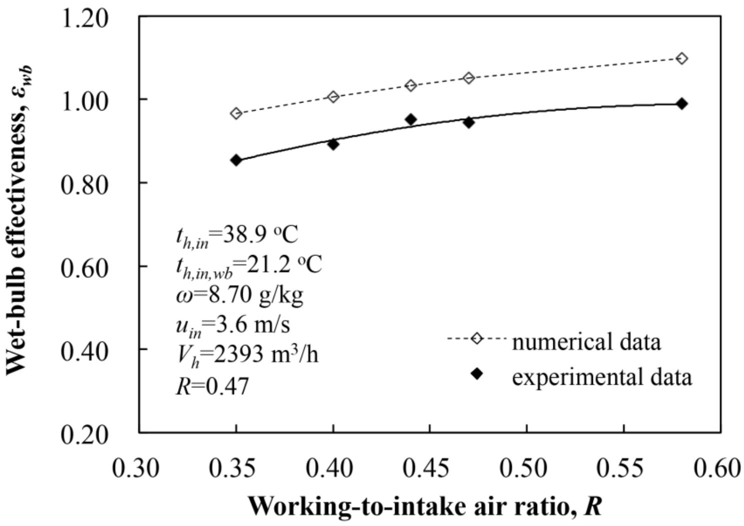

(b)

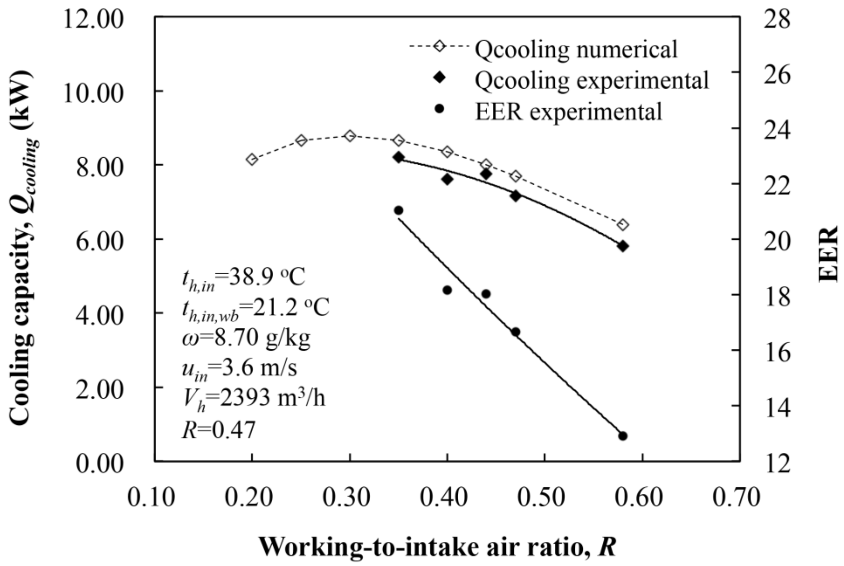

(c)

Fig. 15. Graphs showing the effect of working-to-intake air ratio on the cooler's (a) product air temperature (b) wet-bulb effectiveness (c) cooling capacity and EER

6.4. Comparison with previous experimental studies

To disclose the superior characteristics of the proposed cooler, we evaluated and compare with other regenerative evaporative coolers recently investigated in related experiment studies [16, 19-21] by comprehensively considering operating conditions, geometrical parameters and performance indicators as given in Table 3. Some experimental data were taken from the studies to make comparisons that obtained whilst these regenerative coolers working in certain operating conditions.

To eliminate the effects of different geometries and airflow rates, we examined the cooling capacities of unit volume and unit supply airflow rate of these coolers. It is found that, comparing against the cooler in Ref. [20], the cooling capacity per unit volume provided by the proposed cooler is increased by 62-108%. That means, through conducting an optimisation design on the structure and materials of heat exchanger, the cooling capacity of the presented cooler have been greatly improved with more compact size. Additionally, we noticed that the cooling capacity per unit airflow rate provided by the cooler is similar with those studied in Refs. [16, 19] despite of more humid working condition, but 21.6% higher than that the cooler reported in Ref. [20]. The reason why it has the less cooling capacity per unit airflow rate can be explained by its lower intake air temperature, higher humidity, less working-to-intake air ratio and unmentioned intake air velocity. Besides, while operating at higher intake air velocity, the proposed cooler also achieved similar cooling effectiveness with those of coolers in Refs. [19-21]. Compared to our proposed cooler, the M-cycle cross-flow cooler in Ref. [16] has 17% higher effectiveness due to the much lower supply airflow rate reduced by 86 %. In terms of the energy efficiency, the proposed cooler has the largest EER compared to others.

Table 3. Comparison of regenerative evaporative coolers in recent experimental studies

Parameters	Present study	Ref. [21]	Ref. [20]	Ref. [19]	Ref. [16]
Flow arrangement	Counter flow	Counter flow	Counter flow	Counter flow	M-cycle cross flow
Exchanger dimension (W×H×L), m	0.458×1.08×0.86	0.08×0.045×1.2	0.55×0.69×0.35	0.314×0.594×0.9	0.75×0.6×0.85
Exchanger volume, m^3	0.425	0.004	0.266	0.168	0.383
Channel spacing (dry/wet), mm	3/3	5/5	20/10	6/6	5/5
Channel length, m	0.86	1.2	0.2	0.9	0.85
Channel width, m	0.458	0.08	0.55	0.314	0.75
Total channel numbers	320	9	46	95	131
Intake air temperature, ^oC	35.9-40.1	34	32	36	27.3-41.1

Intake air humidity, g/kg	11.0	11.2	13.6	8.25	7.13-7.9
Intake channel air velocity, m/s	3.6	3.3	N/A	1.58-2.83	N/A
Supply airflow rate, m^3/h	1268	N/A	600	120-257	174-604
Working to intake air ratio	0.47	0.33	0.3	0.5	0.33
Feed water flow rate (g/h)	N/A	60	52.5	N/A	N/A
Supply air temperature, ^oC	22.5-22.8	22	21	20.8-25.6	17.3-19.3
Wet-bulb effectiveness	0.96-1.0	0.96	1.06	0.55-1.06	0.77-1.17
Cooling capacity, kW	5.7-7.3	N/A	2.2	0.68-1.13	1.05-1.22
Cooling capacity per unit volume, kW/m^3	13.4-17.2	N/A	8.27	0.8-6.7	2.7-3.185
Cooling capacity per unit air flow rate, $W/(m^3 \cdot h^{-1})$	4.5-5.8	N/A	3.7	4.3-5.6	2.0-6.0
EER	13.2-17.1	N/A	N/A	10-14	6.8-14.2

7. Conclusions

With increasingly demands for air conditioning in building sectors, this research proposes a large-scale compact regenerative evaporative cooler for buildings as an alternative to conventional compression refrigeration system with great energy saving potential and positive environmental impacts. First, this study optimally designs the structural parameters of the counter-flow heat and mass exchanger by developing a finite element numerical model based on modified ε-NTU method. Subsequently, the heat and mass exchanger was fabricated with a type of evaporation material with high wicking ability, followed by the whole evaporative cooler's construction. Then, the study experimentally examines the cooler's overall performance operating in various conditions controlled by an air-conditioned chamber.

Moreover, the study experimentally and numerically analyses the factors affecting the performance of the cooler including intake air temperature, humidity and velocity and the ratio of working to intake airflow rate. Finally, the proposed cooler is comprehensively compared with other RECs in literature with respect to overall performance, operating and geometrical parameters. Regarding to the above works, some conclusions can be drawn as follows :

1) The developed computational programme can be utilised i) to determine the optimal operating and geometrical parameters of a heat and mass exchanger in regenerative evaporative coolers; ii) to accurately predict the performance of regenerative evaporative coolers, provided that the Lewis relation is satisfied.
2) The experimental results show that the wet-bulb effectiveness of the proposed cooler ranged from 0.96 to 1.07, the cooling capacity and EER varied from 3.9 to 8.5 kW and 10.6 to 19.7 respectively. The cooler can supply cool outlet air temperature below the wet-bulb temperature of inlet air by around 1-2 ^{o}C despite of operating high intake channel air velocities (3.04-3.60 m/s).
3) Through conducting an optimisation design on the structure, material and operating parameters of heat and mass exchanger, the proposed cooler's performance has been greatly enhanced with more compact geometry: Its cooling capacity per unit volume has increased by 62-108%. The cooling capacity per unit airflow rate is either 21.6% higher than a previous counter-flow REC, or comparable with another M-cycle REC.
4) The measured performance is substantially less than that predicted. This discrepancy may be reduced if the feed water mass flow rate was made small in the exchanger while keeping the evaporation surfaces completely wet. Especially, a smaller water mass flow rate should be supplied when the intake airflow rate is small. The water mass flow rate supplied to the heat exchanger should be varied with the intake airflow rate for making further performance optimisation.

Acknowledgements

The authors are grateful to the China and UK scientific research grants funded by Beijing Key Lab of Heating, Gas Supply, Ventilating and Air Conditioning Engineering, Beijing University of Civil Engineering and Architecture, Physical Sciences Research Council (PSRC) and Innovate UK (EP/M507830/1).

References

[1] IEA (International Energy Agency). Energy Balances-2009 ed. Paris, France: International Energy Agency Trans; 2012a.

[2] Tsinghua University Building Energy Research Centre. 2014 Annual Report on China Building Energy Efficiency. Beijing: Tsinghua University; 2014.

[3] Duan Z, Zhan C, Zhang X, Mustafa M, Zhao X, Alimohammadisagvand B, et al. Indirect evaporative cooling: Past, present and future potentials. Renew Sustain Energy Rev 2012;16:6823-50

[4] ASHRAE. ASHRAE Handbook HVAC Systems and Equipment, American Society of Heating, Refrigerating and Air-Conditioning Engineers, 2008.

[5] Maclainecross IL, Banks PJ. A general theory of wet surface heat exchangers and it's application to regenerative evaporative cooling. J Heat Transf 1981;103:579-85.

[6] Hsu ST, Lavan Z, Worek WM. Optimization of wet-surface heat exchangers. Energy 1989;14:757-70.

[7] Zhao X, Li J, Riffat, SB. Numerical study of a novel counter-flow heat and mass exchanger for dew point evaporative cooling. Appl Therm Eng 2008;28:1942-51.

[8] Duan Z, Zhao X, Zhan C, Dong X, Chen H. Energy saving potential of a counter-flow regenerative evaporative cooler for various climates of China: Experiment-based evaluation. Energy Build 2017;148:199-210.

[9] Idalex The Maisotsenko cycle-conceptual. A Technical Concept View of the Maisotsenko Cycle (2003), http://www.idalex.com/technology/how_it_works_-_engineering_perspective.htm.

[10] Anisimov S, Pandelidis D, Jedlikowski A, Polushkin V. Performance investigation of a M (Maisotsenko)-cycle cross-flow heat exchanger used for indirect evaporative cooling. Energy 2014;76:593-606.

[11] Zhan C, Duan Z, Zhao X, Smith S, Jin H, Riffat S. Comparative study of the performance of the M-cycle counter-flow and cross-flow heat exchangers for indirect evaporative cooling – Paving the path toward sustainable cooling of buildings. Energy 2011;36:6790-805.

[12] Ren C, Yang H. An analytical model for the heat and mass transfer processes in indirect evaporative cooling with parallel/counter flow configurations. Int J Heat Mass Transf 2006;49:617-27.

[13] Hasan A. Going below the wet-bulb temperature by indirect evaporative cooling: Aalysis

using a modified ε-NTU method. Appl Energy 2012;89:237-45.
[14] Anisimov S, Pandelidis D. Theoretical study of the basic cycles for indirect evaporative air cooling. Int J Heat Mass Transf 2012;84:974-89.
[15] Heidarinejad G, Moshari S. Novel modeling of an indirect evaporative cooling system with cross-flow configuration. Energy Build 2015;92:351-62.
[16] Jradi M, Riffat S. Experimental and numerical investigation of a dew-point cooling system for thermal comfort in buildings. Appl Energy 2014;132:524-35.
[17] Xu P, Ma X, Diallo TMO, Zhao X, Fancey K, Li D, et al. Numerical investigation of the energy performance of a guideless irregular heat and mass exchanger with corrugated heat transfer surface for dew point cooling. Energy 2016;109:803-17.
[18] Cui X, Chua KJ, Yang WM. Numerical simulation of a novel energy-efficient dew-point evaporative air cooler. Appl Energy 2014;136:979-88.
[19] Duan Z, Zhan C, Zhao X, Dong X. Experimental study of a counter-flow regenerative evaporative cooler. Build Environ 2016;104:47-58.
[20] Lee J, Lee D-Y. Experimental study of a counter flow regenerative evaporative cooler with finned channels. Int J Heat Mass Transf 2013;65:173-9.
[21] Riangvilaikul B, Kumar S. An experimental study of a novel dew point evaporative cooling system. Energy Build 2010;42:637-44.
[22] Zube D, Gillan L. Evaluating Coolerado Corporation's heat-mass exchanger performance through experimental analysis. Int J Energy Clean Environ. 2011;12:101-16.
[23] Frank B. On-site experimental testing of a novel dew point evaporative cooler. Energy Build 2011;43:3475-83.
[24] ASHRAE. ANSI/ASHRAE Standard 143-2015. Method of test for rating indirect evaporative coolers. American Society of Heating, Refrigerating and Air-Conditioning Engineers; 2015.
[25] Pacific Gas and Electric Company. Laboratory evaluation of the coolerado cooler-indirect evaporative cooling unit. Application assessment report #0402 prepared by Pacific Gas and Electric Company Technical and Ecological Services: 2006. p. 10.
[26] The building regulations 2000, Approved document F: Ventilation. Office of the Deputy Prime Minister; 2006.
[27] Incropera PF, DeWitt PD. Fundamentals of heat and mass transfer. 7th ed. New York: John Wiley and Sons; 2011.
[28] Shah RK, London AL. Laminar Flow Forced Convection in Ducts. New York: Academic

Press; 1978.
[29] Klein SA, Alvarado FL. EES-engineering equation solver for Microsoft windows operating systems, user manual, F-Chart software; 2008.
[30] Kakaç S, Shah, RK, and Aung, W. Handbook of Single-Phase Convective Heat Transfer. New York: Wiley; 1987.

Design, fabrication and performance evaluation of a compact regenerative evaporative cooler: towards low energy cooling for buildings

Zhiyin Duan[a*], Xudong Zhao[b], Junming Li[c]

[a] Beijing Key Lab of Heating, Gas Supply, Ventilating and Air Conditioning Engineering, Beijing University of Civil Engineering and Architecture, Beijing 100044, China

[b] University of Hull, Hull, HU6 7RX, UK

[c] Key Laboratory for Thermal Science and Power Engineering of Ministry of Education, Department of Thermal Engineering, Tsinghua University, Beijing 100084, China

Abstract

The urges of reducing energy use and carbon footprint in buildings have prompted the developments of regenerative evaporative coolers (RECs). However, the physical dimensions of RECs have to be designed enormous in order to deliver a large amount of supply airflow rate and cooling capacity. To tackle the issue, this paper develops a large-scale counter-flow REC with compact heat exchanger through dedicated numerical modelling, optimal design, fabrication and experimentation. Using modified ε-NTU method, a finite element model is established in Engineering Equation Solver environment to optimise the cooler's geometric and operating parameters. Based on modelling prediction, the cooler's experimental prototype was optimally designed and constructed to evaluate operating performance. The experiment results show that the cooler's attained wet-bulb effectiveness ranges from 0.96 to 1.07, the cooling capacity and energy efficiency ratio from 3.9 to 8.5 kW and 10.6 to 19.7 respectively. It can provide sub-wet bulb cooling while operating at high intake channel air velocities of 3.04-3.60 m/s. The superiority of proposed cooler's performance is disclosed by comparing with different RECs under similar operating conditions. Both the cooler's cooling capacity per unit volume and per unit airflow rate are found to be 62-108% and 21.6% higher respectively.

Keywords:

Indirect evaporative cooling; Dew point cooling; Heat and mass exchanger; Experimental and numerical investigations

1. Introduction

---

* Corresponding author. Tel: +86 10 68322535

E-mail address: duanzhiyin@bucea.edu.cn (Z. Duan)

Building energy consumption in China had increased by 40% from 1990 to 2009 as the incomes rise and urbanisation advances [1]. The energy consumed by space cooling accounts for around 10% of total building energy use in 2012 [2]. With global warming and rising demand for comfort levels, this share has been increasing continuously. Due to the participations of compressor and refrigerant, the dominant vapour compression refrigeration/air conditioning systems consume large amounts of electrical energy and cause heavy environmental impact. In comparison, Indirect Evaporative Cooling systems (IECs) utilise latent heat of water vaporisation to remove the heat from supply airflow and retain the moisture constant without using compressors and refrigerants that have great potentials in energy saving and associated carbon emissions reduction [3]. However, conventional IECs haven't been widely applied because the ultimate temperature for the IECs' supply air is the wet-bulb temperature of ambient air, which could hardly be achieved in practice. According to Ref. [4], it is thought that only 40 to 80 per cent of temperature difference between ambient air dry-bulb and wet-bulb could be reached in typical indirect evaporative coolers.

Regenerative or Recuperator Evaporative Cooler (REC), as the IECs with closed-loop configuration, has the ability of providing supply air at a temperature below the wet-bulb towards the dew-point temperature of inlet air theoretically [5-7]. According to the estimates [8], a counter-flow REC could annually reduce 13-58% of the total electrical power consumed by conventional compression air conditioners for various climates in China.

Predominantly, there are two types of regenerative evaporative coolers including single-stage counter-flow and multi-stage M-cycle cross-flow configurations [9]. Fig.1 demonstrates the working principles of their basic heat and mass exchanger structure and the psychrometric charts representing thermal process of airflows in dry and wet channels. In the counter-flow regenerative configuration, the intake airflow is circulated through the dry channel, a portion of the airflow is used as cooled product/supply airflow to be delivered to indoors, while being extracted through the perforations, the remaining airflow, as the working air, is re-circulated through the wet channel and is subsequently discarded to the outside. During this thermal process, the product air is cooled along the dry channel without any humidity increase whereas the working air is initially cooled to the minimal temperature with moisture additions at a certain distance from the entrance due to the effect of water evaporation. The temperature of working air subsequently begins to increase with minor moisture increase when the sensible heat transfer from product air in the dry channel exceeds the effect of evaporation cooling [10]. In the remainder of the wet channel, the working air has already reached saturation and has gradually heated under this condition. Eventually, the working air can be heated and humidified towards a temperature a bit higher than the wet-bulb of intake air before it’s exhausted. This counter-flow recirculation arrangement allows the working air to be fully cooled before entering the wet channel, thus leading to increased temperature difference and heat transfer between the working and product airflows.

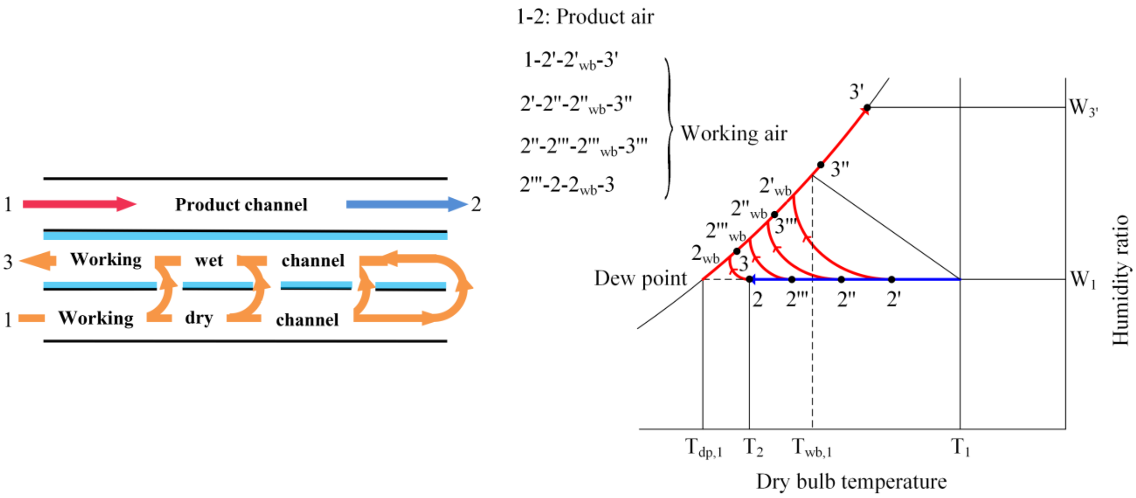

(a)

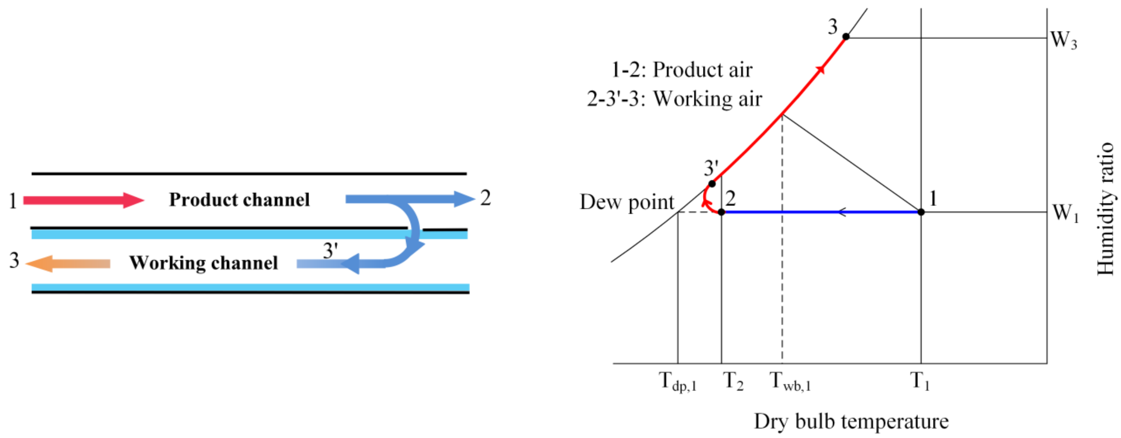

(b)

Fig. 1. Graphs showing working principle and psychrometric process of (a) M-cycle multi-stage regenerative HMX [ref] (b) single-stage regenerative HMX.

In the M-cycle regenerative configuration, part of the dry surface is designed for the product airflow to pass through while the rest is allocated to the working airflow. Both the product and working air flows parallel along the dry channel. A few perforations are evenly distributed over the surface where the working air is contained. Through the small holes, all of the air passing along the working dry channel is gradually diverted to the wet surface, to be used as working air. This portion of airflow is pre-cooled before entering the wet channel by losing heat to the adjacent wet surface. The working air flowing over the wet surface absorbs heat from the product and working air on dry surface. During the thermal process, the product air temperature is reduced with constant moisture, while the working air is partially pre-cooled, humidified and heated in multi-stage process (1-2'-2'wb-3', 2'-2"-2"wb-3", 2"-2'''-2'''wb-3''', 2'''-2-2wb-3) and is finally exhausted to the outside. Compared to the single-stage counter-flow cooler with equivalent physical size and operating conditions, this cross-flow cooler allows the working air to be cooled in multi-stage, thereby leading to 15-23% lower cooling effectiveness and around 20% smaller cooling capacity but 10% higher energy efficiency theoretically [11].

More recently, there have been growing interests on developing the single stage counter-flow and M-cycle regenerative evaporative coolers by analytical, numerical and experimental/field-testing methods. The analytical models being developed are normally based on conventional ε-NTU method when proper alternations are made by redefining the potential gradients, transfer coefficient, heat capacity rate parameters and assuming a linear saturation temperature-enthalpy relation of air. Through making these adjustments, the established analytical models can be used to determine the optimal operating and geometrical parameters of RECs for design problems, as well as to predict or compare the performance of RECs with different airflow patterns including parallel-flow, counter-flow, cross-flow and regenerative flow [10, 12-14]. Usually the analytical models were simplified to achieve acceptable results by making some assumptions, such as: 1) longitudinal thermal conduction in the wall is negligible; 2) Lewis number is unity, 3) heat and mass transfer coefficients inside each channel are constants; 4) water film is uniform and continuous, etc. [5, 13]. By contrast, some sophisticated models can provide more accurate predictions by considering a set of variables including Lewis factor, surface wettability, spray water temperature, and spray water enthalpy change [10, 12].

A few one-dimensional numerical models of counter-flow and two-dimensional models of M-cycle cross-flow RECs have been developed to predict/compare their performance and to analyse the effects of operating and geometrical parameters. The governing differential equations of these models were discretised with finite difference [15, 16] or finite element scheme [7, 11, 17] and solved using Newton iterative method or Eulerian-Lagrangian method [18]. The results of these modelling show that the RECs' performance strongly depends upon the parameters including intake air temperature and humidity, intake air velocity, working-to-intake airflow ratio, channel size of heat exchanger, feed water flow rate and uniformity of water film, but depends less on thermal conductivity of heat transfer sheets and feed water temperature [7, 19].

Additionally, a few experimental/fielding-testing studies have been conducted on counter-flow and M-cycle RECs aiming to 1) validate the numerical or analytical modelling results [16, 20], to 2) study the effects of operating parameters [16, 19, 21], to 3) achieve the internal air temperature and humidity distributions for dry and wet channels [22] and to 4) prove the cooler's technical viability through examining operating performance under various conditions [19, 23]. Most of those regenerative coolers developed are lab scale prototypes that can only provide sub-wet bulb cooling while operating at small intake channel air velocities lower than 1.0 m/s [16, 21]. As the intake air velocity increased from 1.0 to 4.0 m/s, the cooler's effectiveness dramatically declined by nearly 100% [18]. Therefore, to achieve desirable cooing effectiveness or outlet air temperature, the regenerative coolers are suggested to operate under the intake air velocity less than 1.0 m/s. In that case, the physical dimensions of the regenerative coolers have to be designed rather huge in order to deliver a large amount of supply airflow rate or cooling capacity. The question then arises: how to determine the geometric and operating parameters of the heat exchanger for accomplishing the REC optimal performance subject to specified design constraints such as certain cooling requirement and confined geometrical volume.

Aiming at solving the problem, this paper develops a computational model based on modified ε-NTU numerical method to determine the optimal geometrical and operating parameters of a new counter-flow regenerative evaporative cooler designed for buildings. The technical viability of the proposed cooler is confirmed by constructing a dedicated experimental prototype and testing it under various operating conditions in an air-conditioned chamber. The overall performance of the prototype examined in this study includes cooling effectiveness, cooling capacity, and energy efficiency as well as supply air temperature. The cooler's unit performance indicators include cooling capacity per unit volume and per airflow rate. Additionally, the paper experimentally and numerically analyses and compares the factors that affecting the cooler's overall performance, including intake air temperature, humidity, airflow rate and working-to-intake air ratio. To reveal the superior performance of the proposed cooler, the paper finally makes comparisons with those regenerative cooler found in previous studies in terms of overall/unit performance indicators under similar operating conditions.

2. Description of the developed counter-flow regenerative evaporative cooler

As depicted in Fig. 2, the regenerative evaporative cooler developed in this study is a self-contained device, mainly composed of a core heat and mass exchanger, a centrifugal fan, a water distributing/recirculating system and an outer casing. Ambient air is drawn into the cooler by the centrifugal fan, and is primarily filtered before entering the heat exchanger. In the exchanger where the thermal process going through by the process air is equivalent to that shown on the psychrometric charts in Fig. 1(b): The process air consisting of product and working air is cooled along the dry channels without moisture increase and subsequently discharged from the right side. Through the perforations located on the end of channels, a portion of the process air (as the working air) is diverted into the adjacent wet channels. Flowing in counter direction to the process air in dry channels, the working air of wet channels is humidified, heated and finally exhausted to outside. Meanwhile the remainder of process air (as the product air) is purified by a filtration again before it is supplied to outside. A damper was equipped to regulate the ratio of working to product airflow rate. A top water distributor enables water spread evenly across the wet surfaces of heat exchanger. Non-evaporated water is collected in the bottom reservoir and re-circulated to the top reservoir periodically through an electrical pump. When a certain amount of water is consumed, more fresh water is supplied to the top reservoir with a solenoid valve.

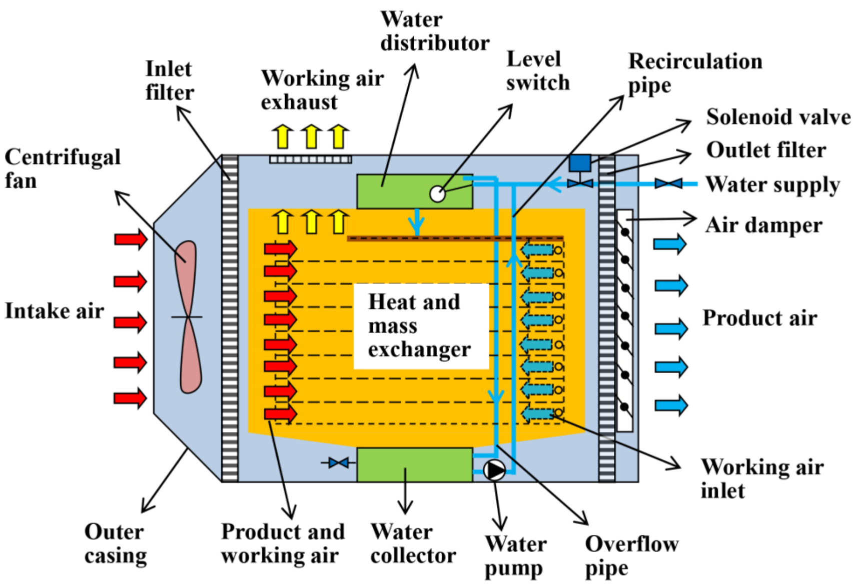

Fig. 2. Schematic diagram of the counter-flow regenerative evaporative cooler

3. Theoretical design of heat and mass exchanger

3.1. Overall and unit performance indicators

Wet-bulb effectiveness of the regenerative cooler, given by Eq. (1), is defined as the ratio of temperature reduction of inlet and outlet air dry-bulb to that of inlet air dry-bulb and wet-bulb.

$$\varepsilon_{wb} = \frac{t_{h,in} - t_{h,out}}{t_{h,in} - t_{h,in,wb}} \tag{1}$$

The cooler's sensible cooling capacity is determined by Eq. (2) derived from ASHRAE Standard 143 [24], when outside ambient air is used as the inlet air.

$$Q_{cooling} = \frac{c_{p,a}\rho_a (V_h - V_c)(t_{h,in} - t_{h,out})}{3.6} \tag{2}$$

Energy Efficiency Ratio (EER) of the evaporative cooler, calculated by Eq. (3), is described as the ratio of sensible cooling capacity to total power consumption of the cooler, i.e. electricity consumption by the air fan and water pump.

$$EER = \frac{Q_{cooling}}{P_{total}} \tag{3}$$

The cooler's unit performance indicators includes cooling capacity per unit volume and per unit airflow rate, which are the sensible cooling capacity determined by Eq. (2) divided by the cooler's geometric volume and supply airflow rate respectively.

3.2. Descriptions of the design problem

The design problem of heat and mass exchanger is complex that involves our comprehensive concerns on the exchanger's intended purpose, geometrical dimensions, capital investment and operating cost. In this study, the following design criteria were considered as a guideline:

- High cooling effectiveness (counter-flow pattern)
- Low pressure drop of airflows, i.e. low fan power consumption
- Compact size of exchanger, i.e. the exchanger's total length and depth are limited within 0.9 and 1.1 m respectively.
- Simple production and construction

To satisfy these needs, we designed a compact counter-flow plate-type heat and mass exchanger. The schematic of the exchanger is shown in Fig. 3. The exchanger comprises a stack of thin cellulose fibre coated plastic sheets, separated by N_{ch} channel gaps. The width (b) and depth (e) of each dry/wet channel gap is set to 3.0 mm and 45.8 mm (>15 times the width) respectively to achieve better heat transfer. The total width of effective heat transfer surface (W) is 0.458 m regardless of the supporting rods between the channels. The thickness of heat exchanger sheets (δ) is 0.375 mm. Therefore, the total depth of exchanger is $H=bN_{ch}+(N_{ch}+1)\delta$. The intake air design temperature is set to $t_{h,in}$ =37.78 °C dry bulb and $t_{h,in,wb}$=21.11 °C wet bulb (Australian standard rating condition, see Ref. [25]). The exchanger is required to provide $Q_{cooling}$=8303 W of cooling capacity with 1530 m^3/h supply/product airflow volumetric rate (V_h-V_c). It's able to supply sufficient air change rate by 1530 m^3/h due to 100% fresh air input, which totally fulfils the demands of the UK's building code [26] (the necessary air change rate for most types of buildings ranges from 4 to 10 ach for 100 m^2 floor area, which is equivalent to 400-1000 m^3/h approximately). Calculated by Eqs. (1) and (2) respectively, the exchanger's wet bulb effectiveness (ε_{wb}) and product air temperature were yield, i.e. ε_{wb}=0.977, $t_{h,out}$=21.5 °C, which are the known parameters for this design problem.

To meet the aforementioned design criteria, the exchanger's optimal geometrical and operating parameters should be determined that incorporate dry/wet channel length and depth (L, H), dry and wet channel numbers (N_{ch}), working-to-intake airflow ratio (R) and intake air velocity or intake airflow volumetric rate (V_h). A numerical computer model based on modified ε-NTU method is developed as follows to accomplish the purpose.

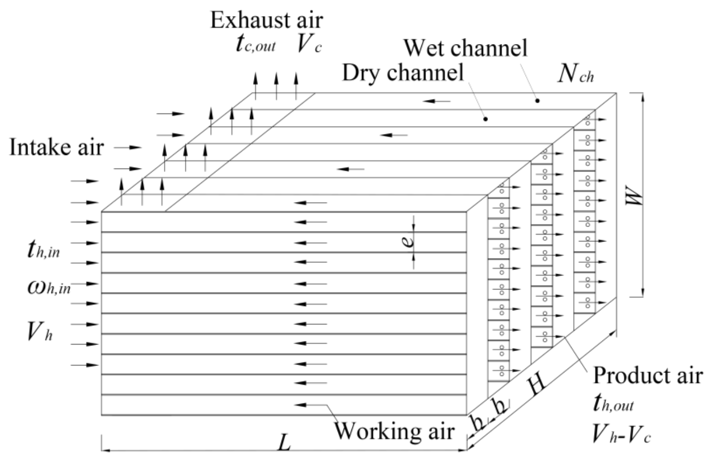

Fig. 3. Schematic of the counter-flow plate-type heat and mass exchanger

3.3. Modified effectiveness-NTU method

3.3.1. Mathematical equations and computational modelling method

The method applied for obtaining a numerical solution to the counter-flow heat and mass exchanger problem is to divide the entire heat exchanger into *N* numbers of computational elements. Fig. 4 illustrates the diagrams of computational element for the numerical modelling with the modified thermal profiles of the entire heat exchanger. A one-dimensional numerical model is developed by applying the modified ε-NTU method to each element of the exchanger and requiring that the boundary conditions associated with each element are consistent with the adjacent element. The numerical problem is coded in Engineering Equation Solver (EES) software and solved by Newton's alternative method. Some assumptions are made to simplify the solutions: 1) the exchanger is assumed to be well insulated to the surrounding; 2) longitudinal thermal conduction in the wall sheet is neglected; 3) fouling resistance of the exchanger is neglected; 4) heat and mass transfer coefficients as well as fluid properties inside each element of the model are constants; 5) Reynolds analogy between heat and mass transfer is valid and the Lewis number is unity; 6) the air-water interface offers a negligible resistance to heat transfer so that the interface temperature is saturated at the water film temperature.

In the modified ε-NTU method, the differential governing equations are directly given below regardless of the mathematical derivation, as the related study is well presented in Ref. [13]. In those equations, proper adjustment is made by redefining some terms stated in typical ε-NTU method, which include: 1) the enthalpy potential gradient for driving the energy transfer between the product air in dry channel and working air in wet channel; 2) the overall heat transfer coefficient and 3) the heat capacity rate parameters.

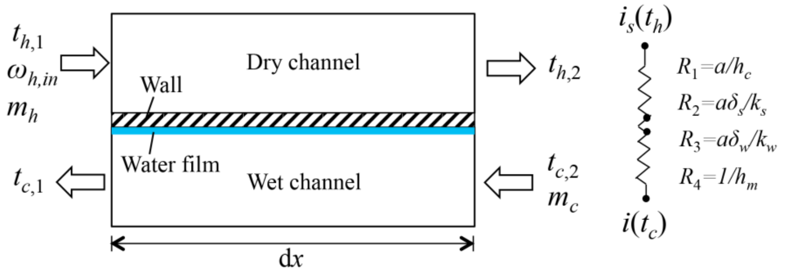

(a)

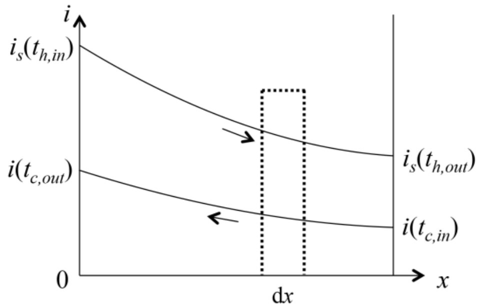

(b)

Fig. 4. Schematic diagrams illustrating (a) computational element for the numerical modelling and (b) modified thermal profiles of the counter-flow heat and mass exchanger

Based on the energy balance on the product air in dry side, the heat transfer rate for each computational element of the exchanger is given by Eq. (4):

$$dq = m_h(i_{h,1} - i_{h,2}) \tag{4}$$

where $i_{h,1}$ and $i_{h,2}$ represent the specific enthalpy of the process/primary air at the inlet and outlet states of each element respectively. An energy balance on the working air in wet side for each element is expressed as Eq. (5):

$$dq = m_c(i_{c,1} - i_{c,2}) \tag{5}$$

where $i_{c,1}$ and $i_{c,2}$ denote the specific enthalpy of the working air at the outlet and inlet states of each element respectively. For the regenerative cooler, the outlet thermal condition of the air in dry channel is equal to the inlet thermal condition of air in wet channel i.e. $i_{h,out} = i_{c,in}$ and $t_{h,out} = t_{c,in}$.

The heat transfer equation between the product air in the dry channel and the working air in the wet channel for the element can be given by Eq. (6):

$$dq = UdA\left(i_s(t_h) - i(t_c)\right) \tag{6}$$

Where the unique enthalpy gradient $i_s(t_h)$-$i(t_c)$ is the driven force making this energy transfer occur. The overall conductance of the heat exchanger is expressed in Eq. (7):

$$UdA = \left(a\left(\frac{1}{h_c} + \frac{\delta}{k} + \frac{\delta_w}{k_w} \right) + \frac{1}{h_m \sigma} \right)^{-1} N_{ch} W dx \tag{7}$$

where σ is the surface wetting factor defined as the ratio of wetting area to the total area of heat transfer, which stands for surface incomplete wetting condition. It varies from 0 to 1 depending on surface wettability, water spraying condition and operating condition. In this study, a typical value of 0.8 was selected for this variable to carry out the modelling [12]. k and k_w symbolise the thermal conductivity of exchanger wall and water film. δ_w represents the thickness of water film, which was assumed to be 0.3 mm.

The enthalpy of air is assumed to have a linear relation with saturation temperature, which can be defined as Eq. (8).

$$i_s(t_h) = a(t_h) + c \tag{8}$$

Where a is the slope of the temperature-enthalpy saturation line and c is a constant in this equation.

The heat capacity rate of primary air (C_h) and secondary/working air (C_c) can be redefined by establishing the heat balance on the air in dry channel and wet channel, which are given in Eqs. (9) and (10) respectively:

$$m_h C_{p,h}(t_{h,1} - t_{h,2}) = C_h \left((i_s(t_{h,1}) - i_s(t_{h,2}) \right) \tag{9}$$

$$m_c C_{p,c}(t_{c,1} - t_{c,2}) = C_c \left(i(t_{c,1}) - i(t_{c,2}) \right) \tag{10}$$

Rearranging the Eq. (9) gives:

$$C_h = m_h C_{p,h} \frac{t_{h,1} - t_{h,2}}{i_s(t_{h,1}) - i_s(t_{h,2})} = \frac{m_h C_{p,h}}{a} \tag{11}$$

Where a can be determined by the ratio of enthalpy difference to the temperature difference between inlet and outlet air in each element of dry channel.

Rearranging the Eq. (10) gives:

$$C_c = m_c \frac{C_{p,c}(t_{c,1} - t_{c,2})}{i(t_{c,1}) - i(t_{c,2})} = m_c \tag{12}$$

The maximum possible heat transfer rate ($q_{\max}$) for the exchanger can be achieved theoretically as the overall conductance (UA) approaches infinity. The fluid with the minimum capacity rate ($C_{\min}$) will experience the maximum possible enthalpy gradient and the maximum heat transfer rate, which can be written as Eq. (13):

$$dq_{\max} = C_{\min} \left(i_s(t_h) - i(t_c) \right) \tag{13}$$

Where $C_{\min,i} = \min(C_h, C_c)$ (14)

The effectiveness of each computational element (ε) is the ratio of the actual heat transfer rate to the maximum possible heat transfer rate:

$$\varepsilon = \frac{dq}{dq_{\max}} \tag{15}$$

Substituting for $dq_{\max}$ from Eq. (13) into Eq. (15) yields:

$$\varepsilon = \frac{dq}{C_{\min} \left(i_s(t_h) - i(t_c) \right)} \tag{16}$$

The number of transfer units and the capacity ratio is expressed as Eqs. (17) and (18) respectively:

$$NTU = \frac{UdA}{C_{\min}} \tag{17}$$

$$C_r = \frac{C_{\min}}{C_{\max}} \tag{18}$$

Where $C_{\max} = \max(C_h, C_c)$ (19)

For a counter-flow exchanger, the effectiveness is determined by Eq. (20) [27]:

$$\varepsilon = \frac{1 - \exp\left[-NTU(1 - C_r)\right]}{1 - C_r \exp\left[-NTU(1 - C_r)\right]} \tag{20}$$

where $C_r<1$

3.3.2. Heat and mass transfer coefficients

In the Eq. (7), the convective heat transfer coefficient (h_c) of the product air in dry channel can be determined as follows. The air velocities in dry and wet channels are calculated by Eqs. (21) and (22) respectively:

$$u_h = \frac{V_h}{0.5WbN_{ch}} \tag{21}$$

$$u_c = \frac{V_c}{0.5WbN_{ch}} \tag{22}$$

Calculating the hydraulic diameter of dry and wet channels yields:

$$D_h = \frac{4 \times b \times e}{2(b + e)} \tag{23}$$

For each computational element of heat exchanger, Reynolds number (*Re*) of the primary and secondary air in dry and wet channels is calculated by Eqs. (24) and (25) respectively:

$$Re_h = \frac{u_h D_h}{\nu_h} \tag{24}$$

$$Re_c = \frac{u_c D_h}{\nu_c} \tag{25}$$

Where ν_h and ν_c denote the kinematic viscosity of process and working air evaluated at average temperature in each element. The Reynolds numbers calculated by above equations are less than 2300, which indicates both the process and working airstreams are laminar flow.

The local convective heat transfer coefficients from process and working air to exchanger walls are decided by Eqs. (26) and (27) respectively:

$$h_{c,h} = \frac{Nu_{T,h} \cdot k_h}{D_h} \quad (26)$$

$$h_{c,c} = \frac{Nu_{T,c} \cdot k_c}{D_h} \quad (27)$$

where k_h and k_c respectively denote the thermal conductivity of process and working air evaluated at average temperature in each element. To obtain the conservative solution, $Nu_{T,h}$ represents the lower bound of local Nusselt number for a laminar, hydrodynamically and thermally fully developed flow in a rectangular duct that is exposed to an uniform wall temperature, which is given by Eq. (28) [28]

$$Nu_{T,fd} = 7.541\left(1 - 2.610(b/e) + 4.970(b/e)^2 - 5.119(b/e)^3 + 2.702(b/e)^4 - 0.548(b/e)^5\right) \quad (28)$$

where b/e=0.066 is defined by the aspect ratio of the minimum to the maximum dimensions of rectangular duct. While the local Nusslet number for a simultaneously developing flow in the rectangular duct as a function of dimensionless position, $L/(D_h RePr)$, was predicted by EES procedure, i.e. DuctFlow_N_local [29], which interpolated a table of data provided by Ref. [30]. Assuming that the Lewis number for air and water mixture is unity, the mass transfer coefficient between working air and water film can be obtained by the following equation:

$$h_m = \frac{h_{c,c}}{C_{p,c}} \quad (29)$$

Where $C_{p,c}$ is the specific heat capacity of moist air assessed at average temperature of working air in each element.

3.3.3. Pressure drop of airflows

The total pressure drop of the process and working air, consisting of friction and minor loss, can be described in Eqs. (30) and (31) respectively.

$$\Delta p_{\text{total},h} = \int_0^L \Delta p_{f,h} + \sum \Delta p_{m,h} \quad (30)$$

$$\Delta p_{\text{total},c} = \int_0^L \Delta p_{f,c} + \sum \Delta p_{m,c} \quad (31)$$

where the friction loss of product air ($\mathbf{\Delta} P_{f,h}$) and working air ($\mathbf{\Delta} P_{f,c}$) in each element are calculated using the Eqs. (32) and (33) respectively [27]:

$$\Delta p_{f,h} = f_h \frac{\rho_h u^2{}_h}{2D_h} dx \quad (32)$$

$$\Delta p_{f,c} = f_c \frac{\rho_c u^2{}_c}{2D_h} dx \tag{33}$$

where the average friction factor (f) of each modelling element is computed by the empirical correlations expressed as Eq.(34) [28], for laminar flow in rectangular duct including the simultaneously developing and fully developed regions.

$$f \approx \frac{4}{\mathrm{Re}}\left[\frac{3.44}{\sqrt{L^+}} + \frac{\frac{1.25}{4L^+} + \frac{f_{fd}\,\mathrm{Re}}{4} - \frac{3.44}{\sqrt{L^+}}}{1 + \frac{0.00021}{\left(L^+\right)^2}}\right] \tag{34}$$

where $L^+=L/(D_h\mathrm{Re})$ is the dimensionless length for a hydro dynamically developing internal flow. The friction factor (f_{fd}) for the fully developed laminar flow in rectangular duct can be determined by the correlation given in Eq. (35) [28]:

$$f_{fd}\,\mathrm{Re} = 96(1 - 1.3553AR + 1.9467AR^2 - 1.7012AR^3 + 0.9564AR^4 - 0.2537AR^5) \tag{35}$$

The minor loss of product and working air in Eqs. (30) and (31) are calculated by Eqs. (36) and (37) respectively:

$$\sum \Delta p_{m,h} = \sum \zeta_h \frac{\rho_h u_h^{\ 2}}{2} = (\zeta_{in,h} + \zeta_{\text{tee,straight}} + \zeta_{filter}) \frac{\rho_h u_h^{\ 2}}{2} \tag{36}$$

$$\sum \Delta p_{m,c} = \sum \zeta_c \frac{\rho_c u_c^{\ 2}}{2} = (\zeta_{\text{tee,branched}} + \zeta_{\text{contraction}} + \zeta_{\text{expansion}} + \zeta_{\text{bend}} + \zeta_{\text{exit}}) \frac{\rho_c u_c^{\ 2}}{2} \tag{37}$$

where $\Sigma\zeta_h$ and $\Sigma\zeta_c$ denote the total minor loss coefficients of the product and working airflow in dry and wet side respectively. $\zeta_{in,h}$ and ζ_{exit} indicate the resistance coefficients for a sharped edged duct inlet and exit respectively. $\zeta_{\text{tee,straight}}$ and $\zeta_{\text{tee,branched}}$ are the resistance coefficients for standard T with flow straight through and primarily through branch respectively. $\zeta_{\text{contraction}}$ and $\zeta_{\text{expansion}}$ represent the resistance coefficients for an abrupt contraction and expansion processes respectively. ζ_{filter} and ζ_{bend} symbolise the resistance coefficients for an air filter and a 90 degree bend.

The actual fan power consumption is the ratio of the total theoretical energy use to the fan efficiency (η), which is given by Eq. (38):

$$P = \frac{\Delta p_{\text{total},h} \cdot V_h + (\zeta_{\text{exit}} + \zeta_{filter}) \frac{\rho_h u_{h,out}^{\ 2}}{2} \cdot (V_h - V_c) + \Delta p_{\text{total},c} \cdot V_c}{\eta} \tag{38}$$

where $u_{h,out}$ =(V_h-V_c)/(0.5WbN_{ch}), which is the outlet air velocity in dry channel.

3.4. Results and discussion of numerical modelling

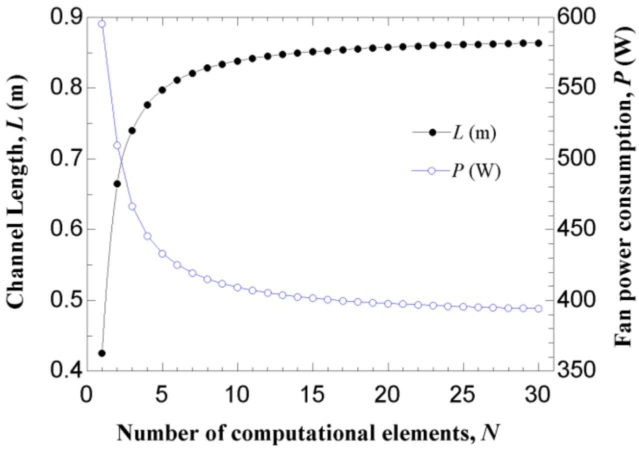

Fig. 5. Channel length and fan power consumption as a function of the number of computational elements

Fig. 5 plots the channel length predicted by the numerical model as a function of the number of computational elements. The result shows that the accurate results of channel length and power consumption can be achieved if the number of computational elements is larger than 20, which are 0.86 m and 394 W respectively.

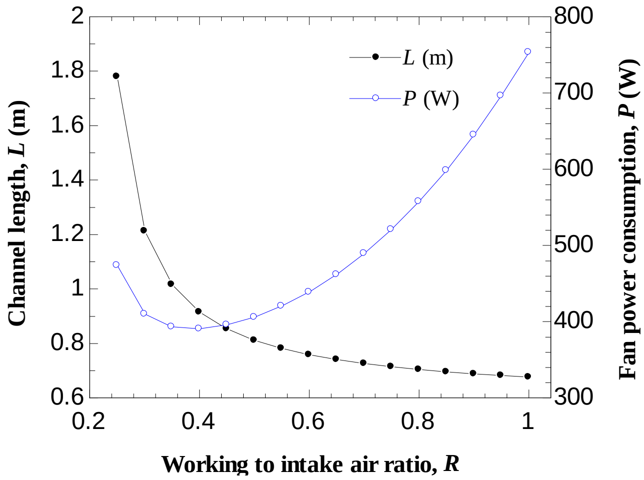

Fig. 6. Channel length and fan power consumption as a function of working-to-intake air ratio

Fig. 6 shows the effects of the ratio of working to intake airflow rate on channel length and fan power consumption. The predicted power consumption reaches minimum with the working-to-intake air ratio varied between 0.35 and 0.45. Also, the predicted channel length drops rapidly with the working-to-intake air ratio smaller than 0.44 and then it gradually decreases without changing too much. Therefore, to reduce the exchanger's capital and operating costs, its working-to-intake air ratio should be set around 0.44.

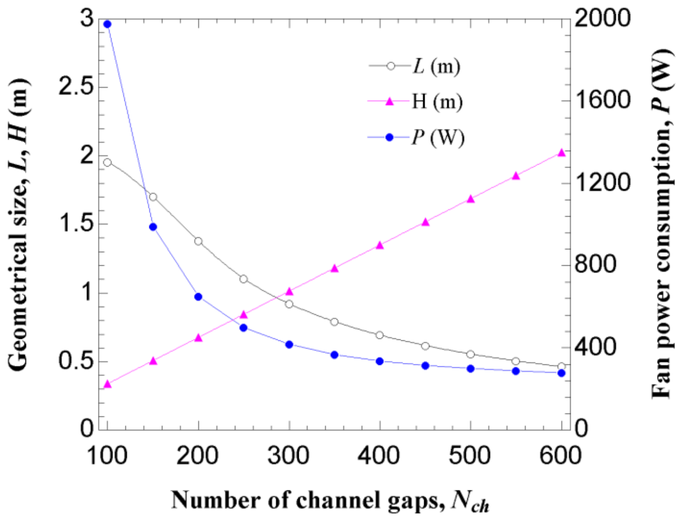

(a)

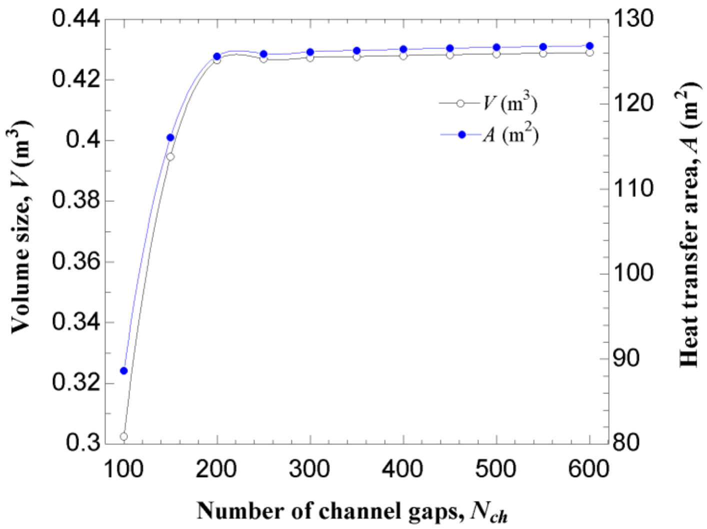

(b)

Fig. 7. Effects of number of channel gaps on (a) channel length, depth and fan power consumption; (b) volume size and heat transfer area of heat exchanger

Fig. 7 indicates the geometrical parameters (channel length and depth) and fan power consumption of the heat exchanger as a function of channel gaps number. With increasing the channel gap number from 100 to 600, the predicted channel length decreases from 1.96 to 0.46 m and the channel depth increases from 0.34 to 2.02 m. Meanwhile, It is shown that the prediction of fan power consumption reduces dramatically with the channel number increasing from 100 to 300 and nearly keeping constant from 300 to 600. The calculated volume size and heat transfer area of the exchanger doesn't vary too much while the channel number increasing from 200 to 600. All in all, the number of 320 channel gaps was determined by comprehensively considering design criteria including simple manufacturing, low energy consumption and limited geometry. The total depth of exchanger is 1.08 m derived from the number of channel gaps. In summary, Table 1 presents the geometrical and operating parameters of the heat exchanger, including the known design conditions and predicted results.

Table 1. Known and predicted design parameters of heat and mass exchanger

Design parameter	Symbol	Unit	Value
Intake air dry-bulb temperature	$t_{h,in}$	°C	37.78
Intake air wet-bulb temperature	$t_{h,in,wb}$	°C	21.11
Intake air humidity ratio	ω	g/kg	9.05
Product air volumetric flow rate	V_h-V_c	m^3/h	1530
Intake air volumetric flow rate	V_h	m^3/h	2737
Cooling capacity	$Q_{cooling}$	W	8303
Fan power consumption	P	W	394
Product air dry-bulb temperature	$t_{h,out}$	°C	21.5
Wet-bulb effectiveness	ε_{wb}	-	0.977
Thickness of thin sheets	δ	mm	0.375
Thickness of water film	δ_w	mm	0.3
Dry/wet channel height	b	mm	3.0
Dry/wet channel width	e	mm	45.8
Dry/wet channel length	L	m	0.86
Total width of heat transfer surface	W	m	0.458
Total depth of the exchanger	H	m	1.08
Thermal conductivity of wall sheet	k	W/(m·K)	0.375
Thermal conductivity of water film	k_w	W/(m·K)	0.3
Fan efficiency	η		0.65
Working-to-intake air ratio	R	-	0.44
Number of dry and wet channels	N_{ch}	-	320

Figs. 8 and 9 respectively depict the effects of channel length and intake airflow rate on overall performance of the cooler while retaining other geometrical and operating parameters the same as shown in Table 1. They indicate that the model developed here can be used to determine the heat exchange's channel length and intake airflow rate if the required cooling effectiveness, cooling capacity and power consumption are known in advance.

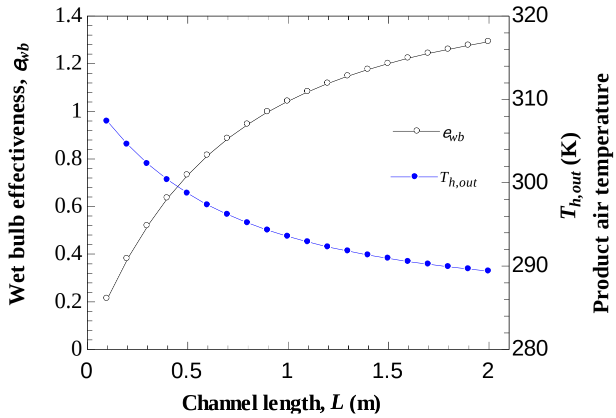

Fig. 8. Calculated wet bulb effectiveness and product air temperature as a function of channel length

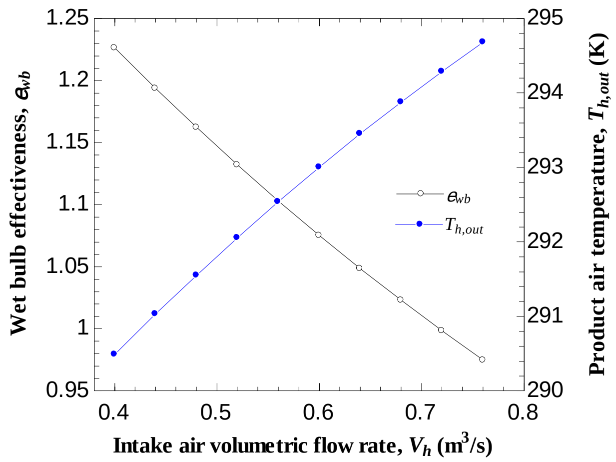

(a)

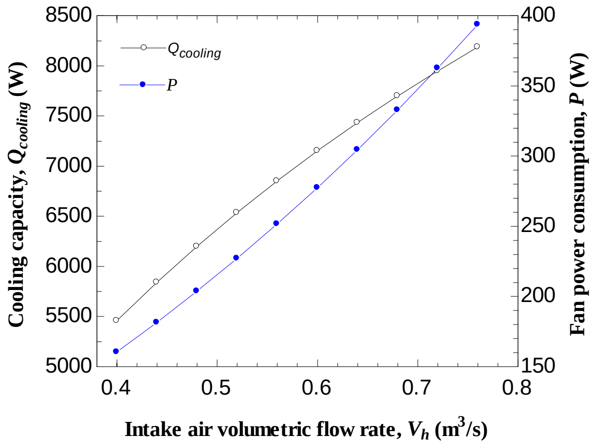

(b)

Fig. 9. Effects of intake air flow rate on (a) wet-bulb effectiveness and product air temperature; (b) cooling capacity and fan power consumption

4. Fabrication of the regenerative evaporative cooler

4.1. Heat and mass exchanger

The heat and mass exchanger was designed, fabricated and constructed as specifications summarised in Table 1. As seen in Fig. 10, the exchanger was stacked together using 160 pairs of dry and wet channels. The dry and wet channels were formed with moisture impervious polymer films and cellulose-blended wicking fibre films, which has superior water absorption and retention abilities compared to other hydrophilic materials [8]. Each dry or wet channel is separated by 10 pieces of long plastic rods having the dimensions of 2×3×860 mm and 2×3×695 mm respectively. These rods were arranged in parallel rows to form long paths with rectangular cross-section (3×45.8 mm), which are designed to guide the passing product and working airflows. Moreover, both two sides of the rods in between wet channels were coated with the same wicking fibre in order to enhance surface wetting condition. Aluminium strips (in 3×10×665 mm) coated with the same wicking fibre material were also constructed at the top of each wet channel to facilitate surface water distribution. It is found that the evaporation surfaces were completely wetted within 5 minutes with assistance of the strips.

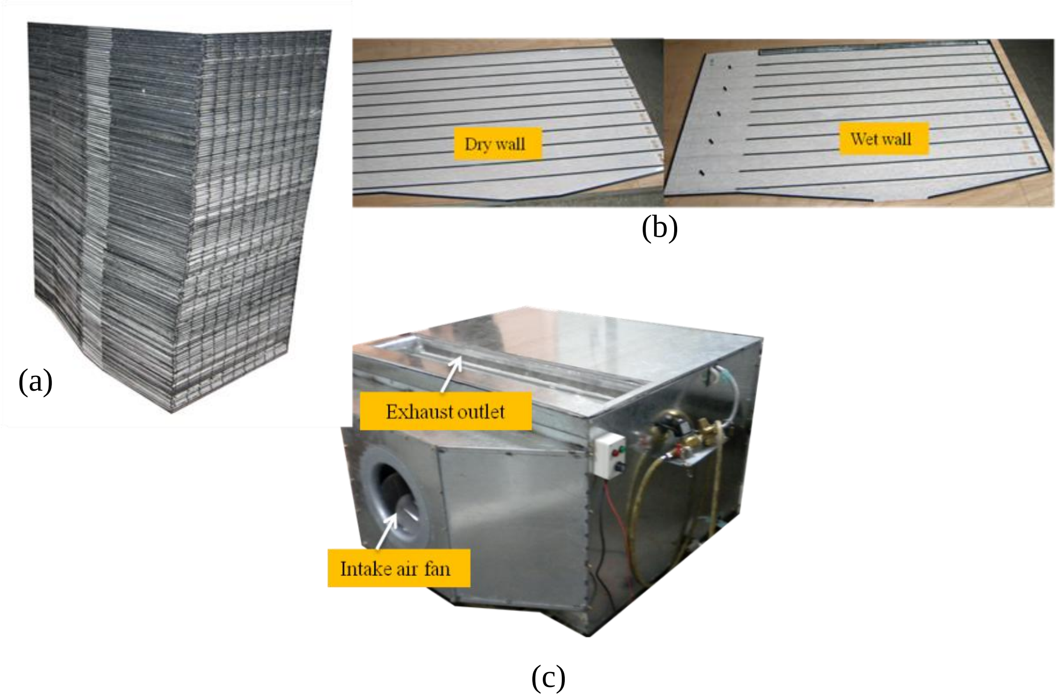

Fig. 10. Photographs showing the fabricated (a) exchanger, (b) dry/wet wall and (c) regenerative evaporative cooler

4.2. Regenerative evaporative cooler

The prototype of regenerative evaporative cooler was mainly assembled using the heat and mass exchanger, a centrifugal fan (manufacturer: ebm-papst, type: K3G355-AI62-06), a water distributor and collector as depicted in Fig. 2. A high efficiency filter made of fibrous materials, being installed between the fan and the inlet of exchanger, is used to remove solid particulates (such as dust, mould and bacteria) from process air and to make the intake air of exchanger distribute more uniformly. Another filter placing at the outlet of heat exchanger, not only to further purify the product air but also to block and divert portions of process air into the adjacent wet channels through the terminal perforations. Evaporation water is supplied from the top water distributor to the top of wet channels through 160 pieces of copper tubes in 2.6 mm outer diameter, located at internals of 6 mm, which is the distance between adjacent wet channels. Unused water is collected in bottom reservoir and recirculated to the top water distributor through an electrical pump (manufacturer: Xin Wei Cheng tech., type: WKA1300-12V). When the water level in the top distributor falls below the lower limit, a water level switch (manufacturer: Cynergy3, type: SSF211X100) can detect the level change and open a joint solenoid valve (manufacturer: COVNA, type: 2W31-15GBN). As a consequence, more fresh water will be supplied to the distributor until the upper limit is reached. The capital cost of the cooling unit was calculated by summing up the prices of the components contained in the unit, taking into account an appropriate rate of labour cost in China. It should be stressed that the prices of the components were quoted from the selected product catalogue and the labour cost was estimated on the basis of mass production premise. Details of the calculation are presented in Table 2.

Table 2. Estimated capital cost of the cooling unit

Component	Unit Price (CNY)	Quantity	Cost (CNY)
Centrifugal fan	10994	1 [piece]	10994
Electrical pump	495	1 [piece]	495
Air filter	100	2[piece]	200
Water distributor	100	1[piece]	100
Water collector	50	1[piece]	50
Solenoid valve	95	1[piece]	95
Supply air damper	80	1[piece]	80
Level switch	570	1[piece]	570
Outer casing	330	1[piece]	330
Heat exchanger	3700	1[piece]	3700
Labour cost	20	80[hours]	1600
Total			18214

5. Experimental set-up

5.1. Experimental instrumentation and measurement method

Fig. 11 demonstrates a layout of the experimental facility for testing the fabricated regenerative evaporative cooler's performance. The cooler was placed in an environmentally controlled room, which is conditioned by an Air Handling Unit (AHU) consisting of a pre-heater, a humidifier, a cooling coil, a re-heater and an air blower. The AHU was adjusted to vary the temperature and humidity of the entering air to the cooler. Both the supply and exhaust airflows of the evaporative cooler were connected to the separate airflow measurement chambers, which are composed of square tunnels with several flow nozzles in the middle. The supply or exhaust airflow rate given in Eq. (39), is obtained by measuring the difference in pressure across the taps at upstream and downstream of the nozzle plate using micro manometers (measurement range：0-1500 Pa, accuracy：0.01 mmH_2O).

$$q_v = CA\sqrt{\frac{2}{\rho}\left(P_1 - P_2\right)} \tag{39}$$

Where, q_v symbolises volumetric flow rate, m^3/s; C denotes orifice flow coefficient, i.e. 0.6, A is the cross-sectional area of the orifice hole, m^2; ρ is the air density, kg/m^3; P_1 and P_2 represent air pressures measured at upstream and downstream of the orifice plate respectively, Pa.

A variable-speed fan located at the outlet of each airflow chambers is used to maintain the required outlet static pressure and compensate for the additional resistance of the pipework and measurement system. The cooler's intake air flow rate was varied by the inlet fan, while its dry-bulb and wet-bulb temperatures were measured by dry-bulb and wet-bulb mercury thermometers (measurement range: -25-50 ^oC, accuracy:±0.2 ^oC) respectively, placed at the inlet of the air cooler. Small portions of the supply airflow were drawn by a blower to a visualised plastic box, where mercury thermometers (measurement range： 0-50 ^oC, accuracy：±0.1 ^oC) were positioned to measure its dry-bulb and wet-bulb temperature. Meanwhile, the cooler's exhaust air dry-bulb and wet-bulb temperatures were tested using the same method. The cooler's energy consumption was gauged using a power meter (measurement range: 0-1000 W, accuracy: ±0.01 W).

The measured data were analysed under steady states, which was defined as the period when the dry-bulb and wet-bulb temperature variations are within 0.1 ^oC for 10 minutes. Once steady state had been achieved, the dry-bulb, wet-bulb temperatures and pressures used for performance analysis were attained by taking algebraic average of the measured data over 10-minute intervals. The data collected enabled a number of performance indicators to be determined including wet-bulb effectiveness, cooling capacity, power consumption and EER.

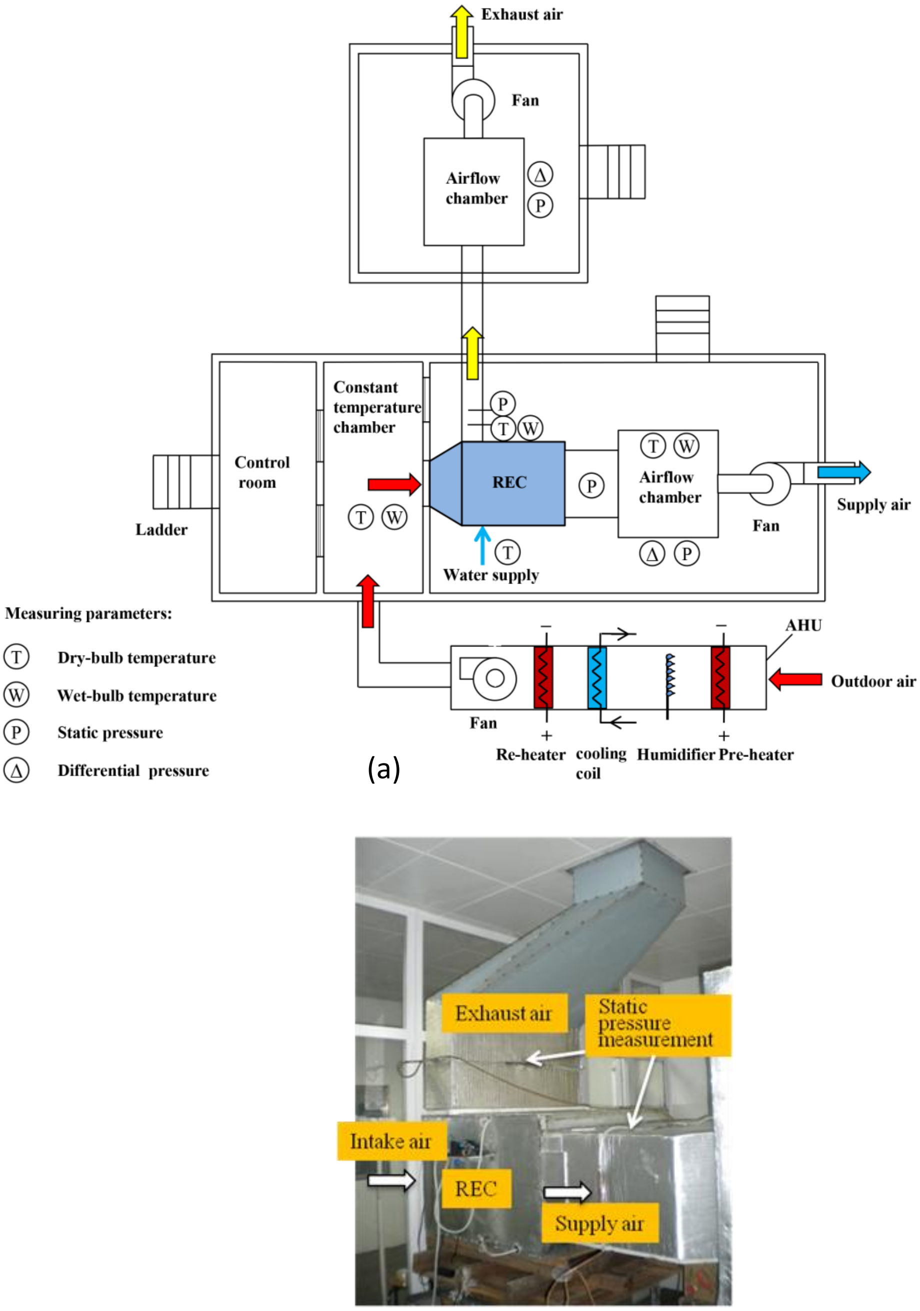

Fig. 11. Graphs showing (a) schematic and (b) photograph of the evaporative cooling system experimental set-up

5.2. Uncertainty analysis of experimental results

The accuracy of experimental results was examined by evaluating energy balance between the cooler's product air and the working air. The energy changes in product and working airflows are determined by Eqs. (40) and (41) respectively. Fig. 12 depicts the comparison of energy changes in product and working air for all experimental data conducted in this work. It is shown that, for most of cases, the energy changes agree well and the inconsistency is below ±10%.

$$E_p = m_1(h_1 - h_2) \tag{40}$$

$$E_w = m_3(h_3 - h_2) \tag{41}$$

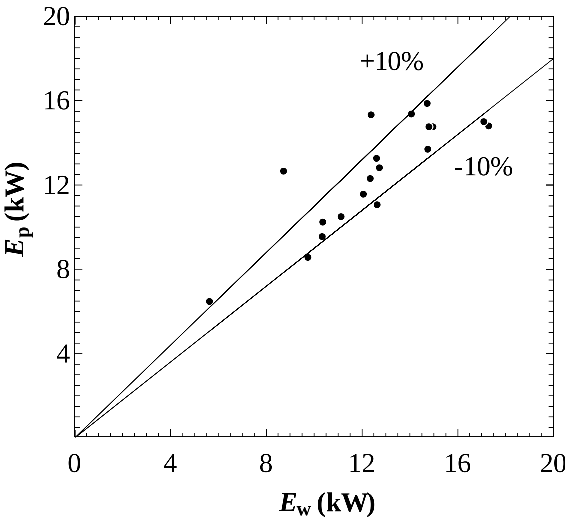

Fig. 12. Comparison between the energy changes in product and working airflows

Eq. (42) was given to calculate the relative uncertainty for the dependent performance indicator variables.

$$\frac{\Delta y}{y} = \sqrt{\sum_i \left(\frac{\partial y}{\partial x_i} \cdot \frac{\Delta x_i}{y}\right)^2} \tag{42}$$

Where $\Delta y/y$ represents the relative uncertainty of dependent variables, i.e. $\Delta\varepsilon_{wb}/\varepsilon_{wb}$, $\Delta Q_{cooling}/Q_{cooling}$, $\Delta EER/EER$; y is the function of the independent variables x_i described in Eqs. (1)-(3) respectively. For instance, $y=\varepsilon_{wb}$, thus $x_i=t_{db,1}$, $t_{db,2}$, $t_{wb,1}$. The uncertainty of airflow rate is determined by pressure drop, given in Eq. (39). The uncertainty for the performance indicator variables was found to be within ±1.31% for wet-bulb effectiveness, ±1.36% for sensible cooling capacity and ±2.61% for EER on average.

6. Performance analysis of the regenerative evaporative cooler

The study experimentally examines the overall performance of the proposed regenerative cooling prototype under various operating conditions and compares the results with the predictions obtained from the aforementioned numerical work. It also analyses the factors that affecting its cooling performance including intake air temperature and humidity, intake airflow rate, and working-to-intake air ratio numerically and experimentally. The achieved results can be employed 1) to analyse the performance of the system in different operating conditions; 2) to optimise its overall performance by determining its appropriate operating parameters; 3) to confirm practicality of the counter-flow cooler applying in hot and dry climates and reveal its novelty characteristics through comparing with previous studies in terms of systems geometrical, operating and performance parameters.

6.1. Effect of intake airflow rate

Fig. 13 shows the cooler's cooling effectiveness, cooling capacity and EER value obtained from the experiment and simulation when gradually increasing the intake airflow rate from 1148 to 2393 m^3/h (corresponding to 1.73-3.60 m/s of intake channel air velocity) while keeping the other operating parameters constant ($t_{h,in}$=38.0 ^oC d.b., $t_{h,in,wb}$=20.8 ^oC w.b., t_w=22 ^oC and R=0.47). It is observed that, for the experimental data, as the intake airflow rate increased by 108%, the cooler's wet-bulb effectiveness declined merely by 7.6% from 1.07 to 0.99 while the supply air temperature increased by 6.6% from 19.6 to 20.9 ^oC. With the same change, the cooling capacity of the system was significantly increased from 3.9 to 7.3 kW by around 84% and the EER from 10.6 to 16.9 by 58.6%. The results show that, when operating under a wide range of intake air velocity (1.73-3.04 m/s), the established prototype could reduce the intake air temperature below its wet-bulb and provide much higher cooling capacity with only a small amount of energy consumption.

It is also found that the discrepancies between the numerical and experimental results ranged from 5.3-19.2%, 3.9-14.4% and 3.9-21.5% in terms of cooling effectiveness, cooling capacity and supply air temperature respectively. The differences are getting larger when intake airflow rate are reduced. For the lowest intake airflow rate, there was biggest gap occurred between the experimental and predicted data. The reason for the increased discrepancy can be explained as follows: For the experiment results, as the intake airflow rate is reduced, the water evaporation rate is getting slower as plotted in the Fig. 11(b) of Ref. [19]. Thus, the ratio of water supplied to water evaporated is getting higher while reducing the intake airflow rate because the water mass flow rate supplied to the exchanger is predominantly constant during the experiment process. The highest water supplied-to-evaporated ratio makes the cooler's effectiveness fall to the lowest level as indicated in the Fig. 6 of Ref. [20]. For the simulation results, however, the uniform and continuous water film is always assumed for all operating conditions without considering excessive water mass flow rate, which could become much larger in the experiment when the intake airflow rate is getting smaller. Therefore, the measured performance is substantially less than that predicted. This discrepancy may be reduced if the feed water mass flow rate was made small in the exchanger while keeping the evaporation surfaces completely wet. Especially, a smaller water mass flow rate should be supplied when the intake airflow rate is small. The similar trend of this discrepancy between measured and predicted effectiveness was also described in the Fig. 3 of an early paper [5], in which assuming that constant water mass flow rate was maintained while varying the air flow rates, the water flow rates would be most excessive and measurements lowest relative to the predictions at low Reynolds numbers, i.e. low air velocities.

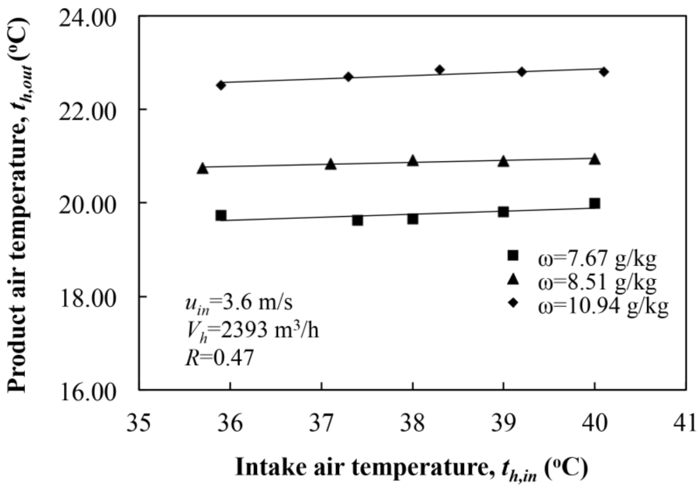

(a)

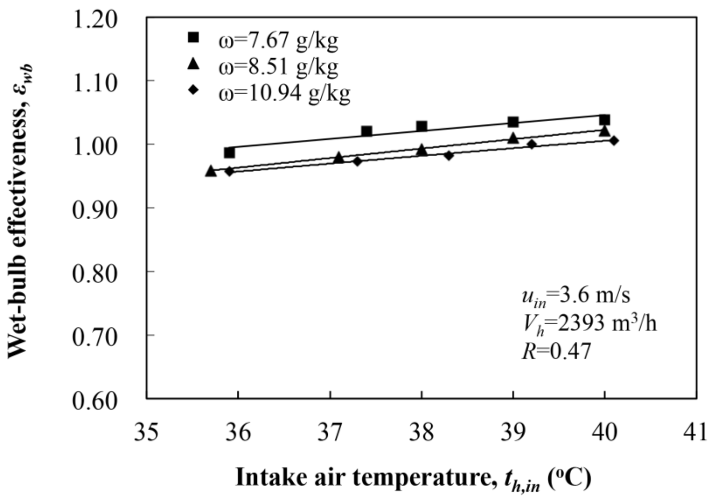

(b)

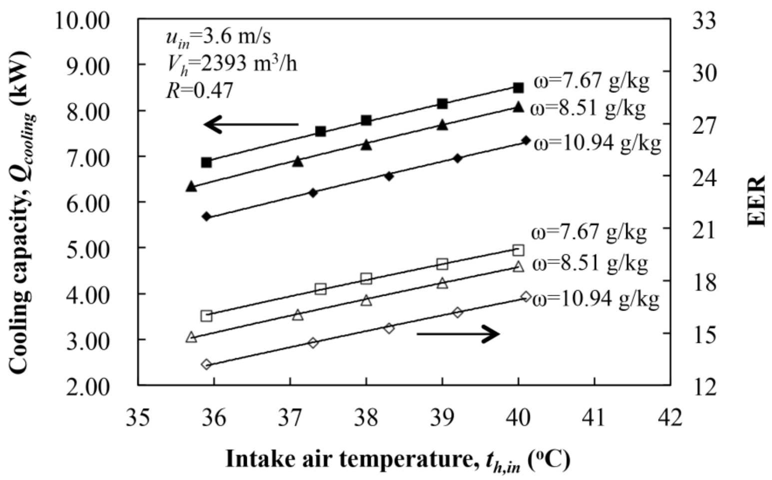

(c)

Fig. 13. Graphs showing the effect of intake airflow rate on the cooler's (a) product air temperature (b) wet-bulb effectiveness (c) cooling capacity and EER

6.2. Effect of intake air temperature and humidity

Fig. 14 depicts the cooler's overall performance evaluated experimentally and numerically under different intake air humidity ratio (ω=7.67, 8.51, 10.94 g/kg) when gradually increasing the intake air dry-bulb temperature from 36 to 40 ^{o}C while retaining the other operating parameters constant (u_{in}=3.6 m/s, V_h=2393 m^3/h, R=0.47, t_w=25.3 ^{o}C). It is found that the cooler's cooling capacity and effectiveness, together with the energy efficiency were linearly growing with increasing the intake air temperature. Operating at highest intake airflow rate, the cooler can achieve 0.96 to 1.04 of wet-bulb effectiveness approximately. The hot intake air can be cooled to 19.7-22.9 ^{o}C (around 1 ^{o}C lower than the wet-bulb temperature of intake air) before it was finally supplied to outside, bring about 13.4-20.0 ^{o}C of temperature reduction. These results indicate the cooling prototype can obtain sub-wet bulb supply air temperature even for the largest intake airflow rate, and it is greatly influenced by the intake air temperature and humidity with respect to the overall performance, as described in Eqs. (1) and (2).

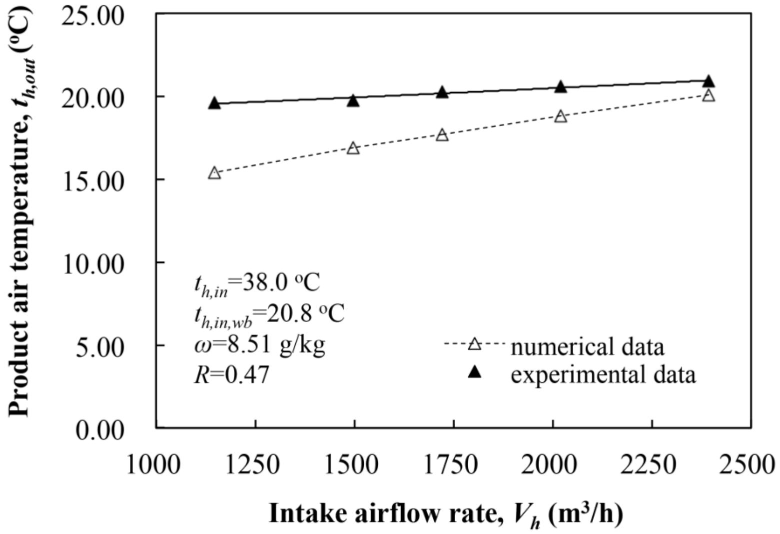
Product air temperature, $t_{h,out}$ (°C)
Intake airflow rate, V_h (m³/h)
$t_{h,in}$=38.0 °C
$t_{h,in,wb}$=20.8 °C
ω=8.51 g/kg
R=0.47
numerical data
experimental data

(a)

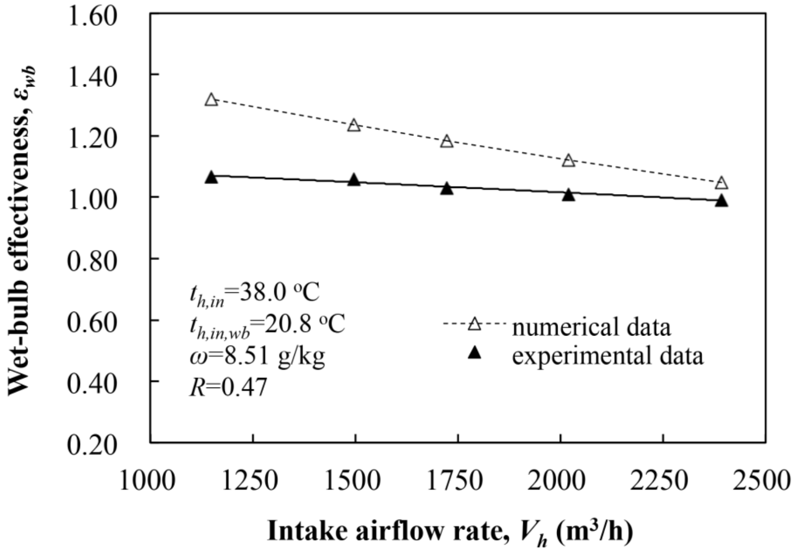
Wet-bulb effectiveness, ε_{wb}
Intake airflow rate, V_h (m³/h)
$t_{h,in}$=38.0 °C
$t_{h,in,wb}$=20.8 °C
ω=8.51 g/kg
R=0.47
numerical data
experimental data

(b)

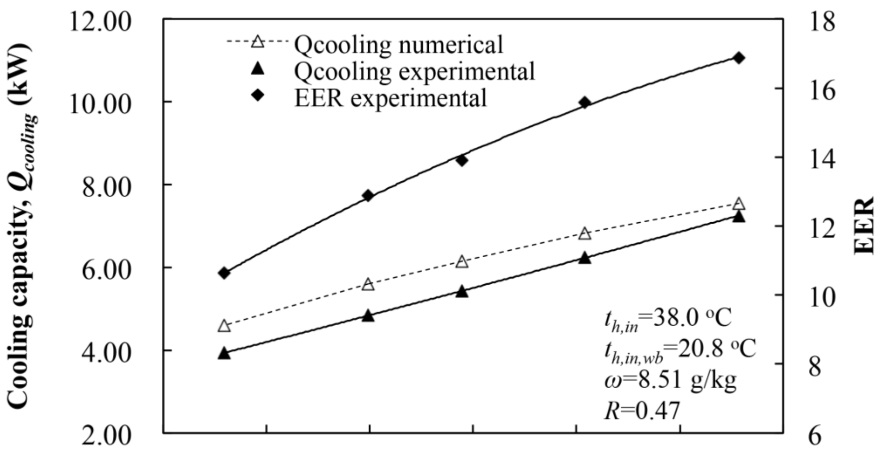
Cooling capacity, $Q_{cooling}$ (kW)
EER
Intake airflow rate, V_h (m³/h)
Qcooling numerical
Qcooling experimental
EER experimental
$t_{h,in}$=38.0 °C
$t_{h,in,wb}$=20.8 °C
ω=8.51 g/kg
R=0.47

(c)

Fig. 14. Graphs showing the effect of intake air temperature and humidity on the cooler's (a) product air temperature (b) wet-bulb effectiveness (c) cooling capacity and EER

6.3. Effect of working-to-intake air ratio

Fig. 15 demonstrates the cooler's overall performance examined experimentally and numerically under different working-to-intake airflow rate ratio while keeping the other operating conditions fixed ($t_{h,in}$=38.9 ^{o}C, $t_{h,in,wb}$=21.2 ^{o}C, V_h=2393 m^3/h, R=0.47). The experimental results show that the working to intake air ratio evidently affects the cooler's overall performance. With the ratio getting higher, the cooler's wet-bulb effectiveness increased by 15.8% from 0.85 to 0.99 and the supply air temperature dropped by 8.4% from 23.7 to 21.7 ^{o}C. Meanwhile, the cooling capacity and EER value enhanced with the ratio increasing from 0.35 to 0.44 and then fell down from 0.44 to 0.58. Hence, considering the contrary variation trends among the wet-bulb effectiveness, cooling capacity and energy efficiency, the optimal ratio of working to intake airflow rate should be around 0.4-0.44.

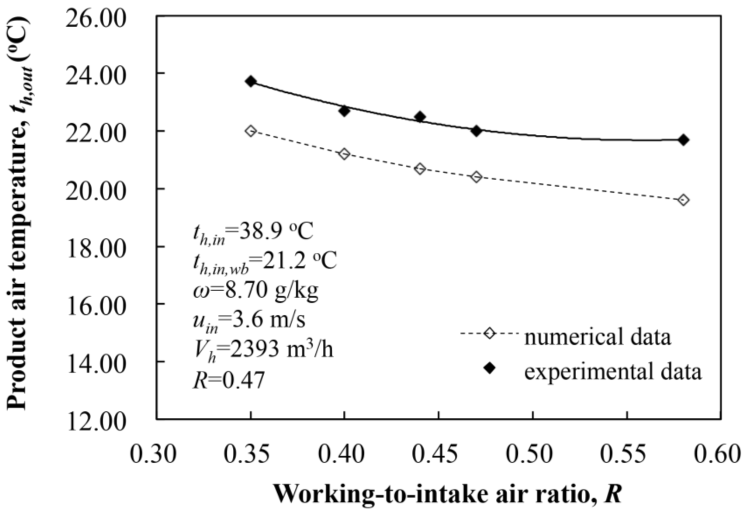

(a)

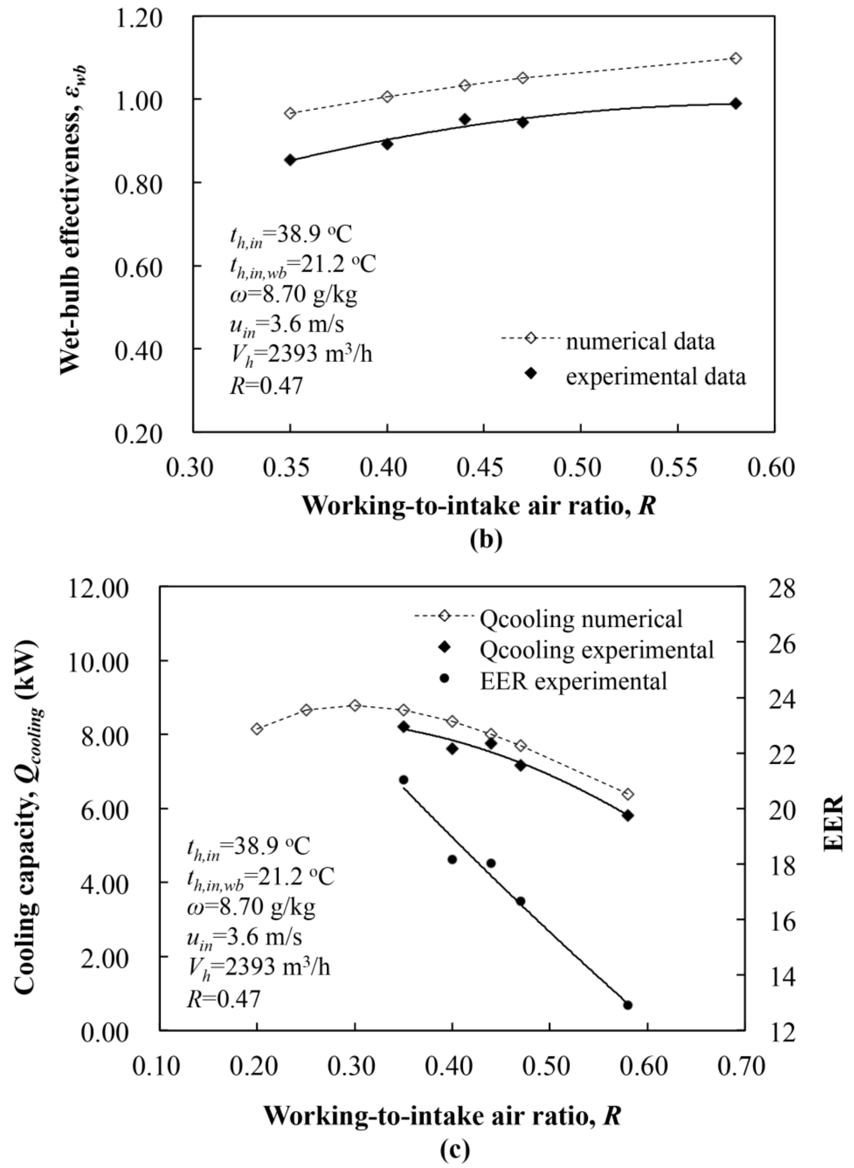

Fig. 15. Graphs showing the effect of working-to-intake air ratio on the cooler's (a) product air temperature (b) wet-bulb effectiveness (c) cooling capacity and EER

6.4. Comparison with previous experimental studies

To disclose the superior characteristics of the proposed cooler, we evaluated and compare with other regenerative evaporative coolers recently investigated in related experiment studies [16, 19-21] by comprehensively considering operating conditions, geometrical parameters and performance indicators as given in Table 3. Some experimental data were taken from the studies to make comparisons that obtained whilst these regenerative coolers working in certain operating conditions.

To eliminate the effects of different geometries and airflow rates, we examined the cooling capacities of unit volume and unit supply airflow rate of these coolers. It is found that, comparing against the cooler in Ref. [20], the cooling capacity per unit volume provided by the proposed cooler is increased by 62-108%. That means, through conducting an optimisation design on the structure and materials of heat exchanger, the cooling capacity of the presented cooler have been greatly improved with more compact size. Additionally, we noticed that the cooling capacity per unit airflow rate provided by the cooler is similar with those studied in Refs. [16, 19] despite of more humid working condition, but 21.6% higher than that the cooler reported in Ref. [20]. The reason why it has the less cooling capacity per unit airflow rate can be explained by its lower intake air temperature, higher humidity, less working-to-intake air ratio and unmentioned intake air velocity. Besides, while operating at higher intake air velocity, the proposed cooler also achieved similar cooling effectiveness with those of coolers in Refs. [19-21]. Compared to our proposed cooler, the M-cycle cross-flow cooler in Ref. [16] has 17% higher effectiveness due to the much lower supply airflow rate reduced by 86 %. In terms of the energy efficiency, the proposed cooler has the largest EER compared to others.

Table 3. Comparison of regenerative evaporative coolers in recent experimental studies

Parameters	Present study	Ref. [21]	Ref. [20]	Ref. [19]	Ref. [16]
Flow arrangement	Counter flow	Counter flow	Counter flow	Counter flow	M-cycle cross flow
Exchanger dimension (W×H×L), m	0.458×1.08×0.86	0.08×0.045×1.2	0.55×0.69×0.35	0.314×0.594×0.9	0.75×0.6×0.85
Exchanger volume, m^3	0.425	0.004	0.266	0.168	0.383
Channel spacing (dry/wet), mm	3/3	5/5	20/10	6/6	5/5
Channel length, m	0.86	1.2	0.2	0.9	0.85
Channel width, m	0.458	0.08	0.55	0.314	0.75
Total channel numbers	320	9	46	95	131
Intake air temperature, ^{o}C	35.9-40.1	34	32	36	27.3-41.1

Intake air humidity, g/kg	11.0	11.2	13.6	8.25	7.13-7.9
Intake channel air velocity, m/s	3.6	3.3	N/A	1.58-2.83	N/A
Supply airflow rate, m^3/h	1268	N/A	600	120-257	174-604
Working to intake air ratio	0.47	0.33	0.3	0.5	0.33
Feed water flow rate (g/h)	N/A	60	52.5	N/A	N/A
Supply air temperature, ^{o}C	22.5-22.8	22	21	20.8-25.6	17.3-19.3
Wet-bulb effectiveness	0.96-1.0	0.96	1.06	0.55-1.06	0.77-1.17
Cooling capacity, kW	5.7-7.3	N/A	2.2	0.68-1.13	1.05-1.22
Cooling capacity per unit volume, kW/m^3	13.4-17.2	N/A	8.27	0.8-6.7	2.7-3.185
Cooling capacity per unit air flow rate, $W/(m^3{\cdot}h^{-1})$	4.5-5.8	N/A	3.7	4.3-5.6	2.0-6.0
EER	13.2-17.1	N/A	N/A	10-14	6.8-14.2

7. Conclusions

With increasingly demands for air conditioning in building sectors, this research proposes a large-scale compact regenerative evaporative cooler for buildings as an alternative to conventional compression refrigeration system with great energy saving potential and positive environmental impacts. First, this study optimally designs the structural parameters of the counter-flow heat and mass exchanger by developing a finite element numerical model based on modified ε-NTU method. Subsequently, the heat and mass exchanger was fabricated with a type of evaporation material with high wicking ability, followed by the whole evaporative cooler's construction. Then, the study experimentally examines the cooler's overall performance operating in various conditions controlled by an air-conditioned chamber.

Moreover, the study experimentally and numerically analyses the factors affecting the performance of the cooler including intake air temperature, humidity and velocity and the ratio of working to intake airflow rate. Finally, the proposed cooler is comprehensively compared with other RECs in literature with respect to overall performance, operating and geometrical parameters. Regarding to the above works, some conclusions can be drawn as follows：

1) The developed computational programme can be utilised i) to determine the optimal operating and geometrical parameters of a heat and mass exchanger in regenerative evaporative coolers; ii) to accurately predict the performance of regenerative evaporative coolers, provided that the Lewis relation is satisfied.
2) The experimental results show that the wet-bulb effectiveness of the proposed cooler ranged from 0.96 to 1.07, the cooling capacity and EER varied from 3.9 to 8.5 kW and 10.6 to 19.7 respectively. The cooler can supply cool outlet air temperature below the wet-bulb temperature of inlet air by around 1-2 ^{o}C despite of operating high intake channel air velocities (3.04-3.60 m/s).
3) Through conducting an optimisation design on the structure, material and operating parameters of heat and mass exchanger, the proposed cooler’s performance has been greatly enhanced with more compact geometry: Its cooling capacity per unit volume has increased by 62-108%. The cooling capacity per unit airflow rate is either 21.6% higher than a previous counter-flow REC, or comparable with another M-cycle REC.
4) The measured performance is substantially less than that predicted. This discrepancy may be reduced if the feed water mass flow rate was made small in the exchanger while keeping the evaporation surfaces completely wet. Especially, a smaller water mass flow rate should be supplied when the intake airflow rate is small. The water mass flow rate supplied to the heat exchanger should be varied with the intake airflow rate for making further performance optimisation.

Acknowledgements

The authors are grateful to the China and UK scientific research grants funded by Beijing Key Lab of Heating, Gas Supply, Ventilating and Air Conditioning Engineering, Beijing University of Civil Engineering and Architecture, Physical Sciences Research Council (PSRC) and Innovate UK (EP/M507830/1).

References

[1] IEA (International Energy Agency). Energy Balances-2009 ed. Paris, France: International Energy Agency Trans; 2012a.

[2] Tsinghua University Building Energy Research Centre. 2014 Annual Report on China Building Energy Efficiency. Beijing: Tsinghua University; 2014.

[3] Duan Z, Zhan C, Zhang X, Mustafa M, Zhao X, Alimohammadisagvand B, et al. Indirect evaporative cooling: Past, present and future potentials. Renew Sustain Energy Rev 2012;16:6823-50

[4] ASHRAE. ASHRAE Handbook HVAC Systems and Equipment, American Society of Heating, Refrigerating and Air-Conditioning Engineers, 2008.

[5] Maclainecross IL, Banks PJ. A general theory of wet surface heat exchangers and it's application to regenerative evaporative cooling. J Heat Transf 1981;103:579-85.

[6] Hsu ST, Lavan Z, Worek WM. Optimization of wet-surface heat exchangers. Energy 1989;14:757-70.

[7] Zhao X, Li J, Riffat, SB. Numerical study of a novel counter-flow heat and mass exchanger for dew point evaporative cooling. Appl Therm Eng 2008;28:1942-51.

[8] Duan Z, Zhao X, Zhan C, Dong X, Chen H. Energy saving potential of a counter-flow regenerative evaporative cooler for various climates of China: Experiment-based evaluation. Energy Build 2017;148:199-210.

[9] Idalex The Maisotsenko cycle-conceptual. A Technical Concept View of the Maisotsenko Cycle (2003),
http://www.idalex.com/technology/how_it_works_-_engineering_perspective.htm.

[10] Anisimov S, Pandelidis D, Jedlikowski A, Polushkin V. Performance investigation of a M (Maisotsenko)-cycle cross-flow heat exchanger used for indirect evaporative cooling. Energy 2014;76:593-606.

[11] Zhan C, Duan Z, Zhao X, Smith S, Jin H, Riffat S. Comparative study of the performance of the M-cycle counter-flow and cross-flow heat exchangers for indirect evaporative cooling – Paving the path toward sustainable cooling of buildings. Energy 2011;36:6790-805.

[12] Ren C, Yang H. An analytical model for the heat and mass transfer processes in indirect evaporative cooling with parallel/counter flow configurations. Int J Heat Mass Transf 2006;49:617-27.

[13] Hasan A. Going below the wet-bulb temperature by indirect evaporative cooling: Aalysis

using a modified ε-NTU method. Appl Energy 2012;89:237-45.
[14] Anisimov S, Pandelidis D. Theoretical study of the basic cycles for indirect evaporative air cooling. Int J Heat Mass Transf 2012;84:974-89.
[15] Heidarinejad G, Moshari S. Novel modeling of an indirect evaporative cooling system with cross-flow configuration. Energy Build 2015;92:351-62.
[16] Jradi M, Riffat S. Experimental and numerical investigation of a dew-point cooling system for thermal comfort in buildings. Appl Energy 2014;132:524-35.
[17] Xu P, Ma X, Diallo TMO, Zhao X, Fancey K, Li D, et al. Numerical investigation of the energy performance of a guideless irregular heat and mass exchanger with corrugated heat transfer surface for dew point cooling. Energy 2016;109:803-17.
[18] Cui X, Chua KJ, Yang WM. Numerical simulation of a novel energy-efficient dew-point evaporative air cooler. Appl Energy 2014;136:979-88.
[19] Duan Z, Zhan C, Zhao X, Dong X. Experimental study of a counter-flow regenerative evaporative cooler. Build Environ 2016;104:47-58.
[20] Lee J, Lee D-Y. Experimental study of a counter flow regenerative evaporative cooler with finned channels. Int J Heat Mass Transf 2013;65:173-9.
[21] Riangvilaikul B, Kumar S. An experimental study of a novel dew point evaporative cooling system. Energy Build 2010;42:637-44.
[22] Zube D, Gillan L. Evaluating Coolerado Corporation's heat-mass exchanger performance through experimental analysis. Int J Energy Clean Environ. 2011;12:101-16.
[23] Frank B. On-site experimental testing of a novel dew point evaporative cooler. Energy Build 2011;43:3475-83.
[24] ASHRAE. ANSI/ASHRAE Standard 143-2015. Method of test for rating indirect evaporative coolers. American Society of Heating, Refrigerating and Air-Conditioning Engineers; 2015.
[25] Pacific Gas and Electric Company. Laboratory evaluation of the coolerado cooler-indirect evaporative cooling unit. Application assessment report #0402 prepared by Pacific Gas and Electric Company Technical and Ecological Services: 2006. p. 10.
[26] The building regulations 2000, Approved document F: Ventilation. Office of the Deputy Prime Minister; 2006.
[27] Incropera PF, DeWitt PD. Fundamentals of heat and mass transfer. 7th ed. New York: John Wiley and Sons; 2011.
[28] Shah RK, London AL. Laminar Flow Forced Convection in Ducts. New York: Academic

Press; 1978.
[29] Klein SA, Alvarado FL. EES-engineering equation solver for Microsoft windows operating systems, user manual, F-Chart software; 2008.
[30] Kakaç S, Shah, RK, and Aung, W. Handbook of Single-Phase Convective Heat Transfer. New York: Wiley; 1987.